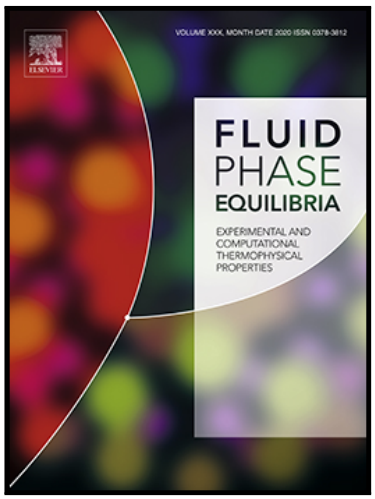

A classification of phase envelopes for reservoir fluids with Asphaltene onset lines: Exploring topology transitions based on compositional changes

Federico E. Benelli , Gerardo O. Pisoni , Martin Cismondi-Duarte

PII: S0378-3812(23)00194-2
DOI: https://doi.org/10.1016/j.fluid.2023.113914
Reference: FLUID 113914

To appear in: *Fluid Phase Equilibria*

Received date: 19 May 2023
Revised date: 27 July 2023
Accepted date: 6 August 2023

Please cite this article as: Federico E. Benelli , Gerardo O. Pisoni , Martin Cismondi-Duarte , A classification of phase envelopes for reservoir fluids with Asphaltene onset lines: Exploring topology transitions based on compositional changes, *Fluid Phase Equilibria* (2023), doi: https://doi.org/10.1016/j.fluid.2023.113914

A classification of phase envelopes for reservoir fluids with Asphaltene onset lines: Exploring topology transitions based on compositional changes

Federico E. Benelli[1], *Gerardo O. Pisoni*[1], *and Martin Cismondi-Duarte*[*†1]

[1]*Instituto de Investigación y Desarrollo en Ingeniería de Procesos y Química Aplicada (IPQA), Facultad de Cs. Exactas Físicas y Nat., Universidad Nacional de Córdoba (UNC)−Consejo Nacional de Investigaciones Científicas y Técnicas de la República Argentina (CONICET), Avenida Velez Sarsfield 1611, Ciudad Universitaria, X5016GCA Córdoba, Argentina.*

Abstract

Reservoir fluids may present complex phase diagrams involving three-phase behavior, due to the presence of different compounds that -when exceeding certain quantities- can induce the separation of a second liquid phase. Typical and important cases are carbon dioxide, water, and asphaltenes, while the mere asymmetry in the mixture of hydrocarbons can also be responsible for a three-phase region in the fluid phase envelope. Although the behavior and practical implications are quite different in each of these cases, their phase diagrams may share some qualitative characteristics and therefore require similar methods and strategies for their calculation. A general calculation strategy, which includes details about the calculation method for certain types of three-phase envelopes and emphasizes the importance of double saturation points, was presented in a previous publication. The main objective of this study is to explore the different possible topologies that the phase envelope of a reservoir fluid may adopt as a result of compositional changes, when using an equation of state (EOS). Reference fluids (compositional data and parameters) were taken from the literature. Based on these fluids, different alterations in the amounts of defined or pseudo-components of the system were used to analyze their effect on the predicted phase diagram. A new type of behavior was identified, which is included in a classification that currently consists of four different types. Additionally, a complete and updated algorithm is presented, which enables the computation of the different topologies presented in this study. Finally, it is shown that transitions between different types of phase diagram can be observed not only as a consequence of compositional changes but also based on modeling or parametric changes in the description of a given fluid, for example by changing the lumping strategy for the heavy fractions.

Keywords: *phase envelopes; asphaltenes onset lines; phase behavior classification; gas injection; phase diagram computation*

[†]Corresponding author: martin.cismondi@unc.edu.ar

1. Introduction

After decades of experience, it is well known both in industry and academia that asphaltenes can create different types of problems in the production, transport, and processing of reservoir fluids, from the reservoir rock to the refinery, and including of course intermediate stages with different facilities and pipes in between [1]. It is also clear that the study of asphaltenes brings complexities of different types to be dealt with, from their very definition and molecular diversity to their phase behavior at high or low pressures, the complex mechanisms going from aggregation in solution to deposition and their discussed reversibility [2–6], not to mention other aspects like their role in the stabilization of water-oil emulsions. Nevertheless, despite all those complexities and discussions associated, there are different reasons to consider precipitated asphaltenes as a heavy liquid phase, at least in the first step when asphaltenes come out of solution, forming particles of an asphaltenic denser phase. First of all, considering the polydispersity and molecular diversity of asphaltenes, it is evident that -contrary to what happens with paraffins- asphaltenes do not form solid crystalline structures. In a more practical or pragmatic view, maybe the most important reason is simply that, after many experimental studies providing measurements of asphaltene onset pressure (AOPs), it is clear that these lines behave in the pressure-temperature space as liquid-liquid saturation lines, which may also have continuity with dew lines at high temperatures. In addition, the majority liquid phases rich in asphaltenes can be observed directly, for example, in solvent diluted bitumens [7]. Then, it is natural to model these fluids and behaviors with equations of state, either cubic, SAFT or other types, as it has been done by different research groups for the last two decades or more [1,8,9] and it is also the modeling approach implemented in different commercial PVT simulators.

Moreover, several published works have studied the effect of certain compositional changes, especially gas injection, on the AOP and bubble pressure lines. Gonzales et al. [10] studied the gas-induced asphaltene precipitation in a live oil and a dead oil, simulating the injection of different gasses (N_2, CO_2, CH_4) using the PC-SAFT EOS. The authors showed how the AOP and the bubble pressure curve (BP) shift considerably, modifying the pressure range in which the precipitation phenomenon occurs when the concentration of any of these gasses increases (or is incorporated, as in the case of dead oil) with respect to the reference composition. In particular for CO_2 and based on model predictions, it is stated that it can increase or decrease the solubility of asphaltenes depending on the characteristics of the fluid and the temperature. Panuganti et al. [11] studied the behavior of the AOP lines calculated with PC-SAFT EoS, with focus on the lower AOP, for three different crude oils (A, B and C). Based on their characterization of fluids and modeling results, the authors conclude that cubic equations of state -in particular, SRK- are less accurate than PC-SAFT for predicting changes in the AOP curve when the injection of light gases into the studied crude oil is simulated. Similar works were carried out by Arya et al. [12–15], using mainly the CPA model. In those works, besides studying the effects of association as well as of different inputs like SARA information in order to develop a modeling and parameterization approach, the authors investigated the effect of injecting light gases (particularly CO_2, N_2, and methane) on the AOP and bubble pressure curves for different types of fluids. The results show different types of transitions in limited pressure and temperature ranges of interest. Other works have also emphasized that the profile of the damaged area by asphaltene deposition is governed by the shape of the asphaltene precipitation envelope for the reservoir fluid, integrating the compositional model in a reservoir simulator to study the dynamics of precipitated asphaltenes [16].

Despite the different interesting analysis, conclusions and methodologies contributed by those and other works available in the literature, covering both modeling and application aspects, clear gaps can be noted concerning two other important and related aspects:

1- No published work presented complete phase envelopes, including the different two and three-phase boundaries involved for these types of fluids. Moreover, none of the considered works detailed or exposed any type of calculation methodology or algorithmic procedure employed for computing the

equilibrium lines. Based on personal communications with different groups and colleagues, we know that in most cases the temperature-pressure space is scanned with a multiple-phase flash, in order to find the conditions for an AOP or bubble pressure, which is cumbersome, inefficient, and time consuming.

2- None of the reviewed studies proposed a classification or even discussed or considered the possible topologies for the complete phase diagrams of reservoir fluids with asphaltene AOP curves, and neither attention has been paid to transitions between different types of arrangements and what may cause them.

While a previous work [17] was devoted to fill the first gap, the present is focused on the second. So, let us first review that previous work, which was focused on developing a general and efficient method for tracing phase envelopes of reservoir fluids that include asphaltene onset pressures, predicted from an equation of state.

1.1 The original algorithm

The developed algorithmic strategy to trace these complex phase envelopes, summarized schematically in Figure 1, could be simplified into three steps or stages:

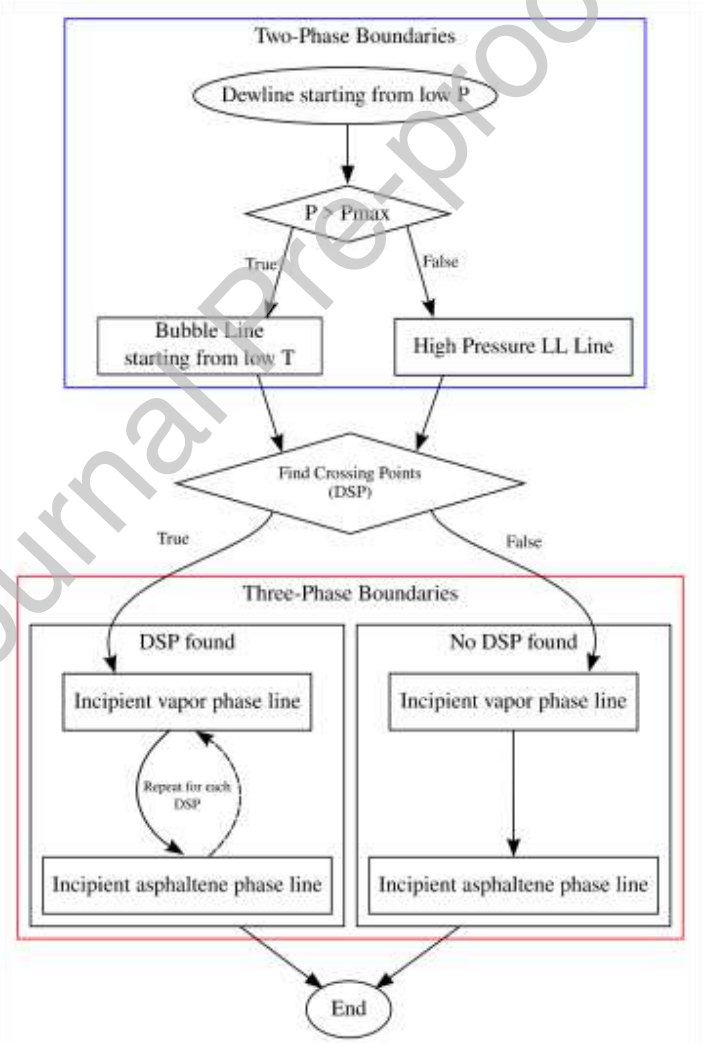

Fig. 1 Original algorithmic strategy, as proposed by Cismondi (2018)

(1). Two-phase boundaries: Compute different possible biphasic phase envelope sections (two-phase boundaries) starting from different points.

(2). Crossings: Detect crossings, if any, between the calculated biphasic lines. Discard internal unstable segments.

(3). Three-phase boundaries: Compute three-phase boundary lines, using initializations depending on the crossings detection.

In this way, the proposed method saves computing time by avoiding the necessity of a stability analysis at each point during the biphasic lines calculations, thanks to the detection and elimination of unstable regions after the lines have been traced.

In the first stage, the first biphasic saturation line to be calculated is always the one starting from a low-pressure dew point. Then, it depends on how that first line progresses in the P-T space: In case it diverges to high pressures, passing a preset maximum value Pmax (the most frequent situation) then the second line will start from a low-temperature (false) bubble point. But if the first line closes itself as a simple and typical phase envelope going to lower temperatures along the bubble side, without having reached Pmax, then the second line should start from a liquid-liquid saturation point at Pmax. In any case, we will end up with two different biphasic saturation lines calculated.

After both lines have been traced, a search for crossings between them is made, where two possible scenarios could arise:

A. Both lines never cross each other

In this case, the inner line (the one started from the low-temperature bubble side) is totally unstable so it is discarded. After that, two different three-phase boundaries are calculated, taking data from the first converged point of the unstable biphasic line for initialization, specifically its pressure and the fugacity coefficients in the liquid phase, which are used to calculate the separation factors as follows:

$$K_i^S = \frac{\phi_i^F}{\phi_i^{Asph}}$$

where the superscripts *F* and *Asph* correspond to the liquid phase of the unstable bubble point and a pure asphaltene phase, respectively. After that first three-phase boundary has been completed, a second and inner line is traced, this time one in which the incipient phase is asphaltenic, i.e. the one known as lower AOP. To initialize this line a search is made, starting from the temperature of the first converged point of the biphasic bubble line and then making pressure decrements and temperature increments until the fugacity of the heaviest compound (asphaltenes) in the heaviest phase taken from a standard liquid-vapor flash calculation is equal to the fugacity of the pure compound at the same conditions.

B. There are crossings between both biphasic lines

A crossing between the dew line and bubble line infers that there is a point with two incipient phases, hence there is a transition from a monophasic region to a three-phase one. This point is referred to as a double saturation point (DSP). In this case, the boundaries delimiting the three-phase region departing from each DSP are calculated using information from that DSP as initialization, in particular the K-factors of the bubble and dew biphasic lines to initialize the light and heavy incipient phases respectively.

In all cases, any biphasic boundary located in the region inside another biphasic boundary is considered unstable, so it must be discarded. It is important to remark that the computing methods for tracing either two or three-phase boundaries are based on sensitivities, as developed originally by Michelsen for two-phase envelopes of multicomponent fluids [18] and then adapted for example to different types of curves in binary systems [19–21]. This way, the calculation proceeds automatically, specifying for each new point the variable with the highest sensitivity, i.e. the variable which changes faster at that point of the envelope. Figures explaining the tracing process can be found in Appendix C.

In that previous work [17], three different fluids were chosen as case-studies. Two of them presented crossings, but leading to different topologies, while the other did not show any crossing or DSP (situation A described above).

Some questions that naturally arose after that work are the following:

- Which other topologies could be obtained for the complete phase envelopes of this type of systems?
- How should we classify those phase diagrams?
- How should the algorithm be extended in order to consider all types?
- How are the transitions between the different topologies and which compositional changes promote each of them?

This new work focuses on providing answers to those questions. In order to do this, an exploratory analysis has been performed, taking as a starting point the same three cases already studied in the previous work, but making compositional variations. Based on topology differences found with these variations, an initial categorization in four unique types was made. Also, some special cases among these types were found that required an extension of the previously developed algorithm.

2. Approach and Methodology

Given that the three fluids considered in the previous work together with their corresponding adopted compositional models gave place to three different topologies, in this new study we take them as departure reference cases. We will apply different compositional changes to each of them, essentially injection of (or dilution in) methane, CO_2, H_2S, asphaltenes and intermediate compounds. The compositions of the three original fluids are shown in Table 1. The agreement between measured and predicted AOPs for cases 2 and 3 can be seen in references [9] and [17].

The idea is to find out which compositional changes can lead to qualitative changes in the predicted phase diagram, how these transformations proceed and whether the modified behaviors would correspond to another previously considered topology or to a new one that should be considered as well. If necessary, considering a new type of diagram, or even a new way of arriving at one of the already obtained types, will require to adapt the original algorithmic strategy discussed in the previous work. The compositional changes were made by proportional additions and removals, in moles, of the selected component and later renormalization of the whole fluid mixture.

Just as an example of the compositional changes implemented, Table 2 presents some detailed compositions when analyzing methane removal/injection to Case 3, including the original composition and also some variations considered in this study. From here on, we will simply use the +/- X% notation, to be interpreted just as in these examples.

Table 1. Characterized compositions of the three originally studied cases.

Component	Case 1
CO2	0.0246
C1-N2	0.3694
C2-C3	0.0752
C4	0.0193
C5	0.0157
C6	0.0162
C7+n	0.47145
Asph	0.00815
Experimental	Burke et al. [22]
Characterized	Gonzalez et al. [25]
EoS	PR78 [26]

Cinoibebt	Case 2	Case 3
N2	0.0049	0.0048
CO2	0.11369	0.00919
H2S	0.0322	--
C1	0.27357	0.43391
C2	0.09409	0.1101
C3	0.06699	0.06544
iC4	0.0081	0.00789
nC4	0.0317	0.03787
iC5	0.0122	0.01279
nC5	0.0198	0.02248
C6	0.0249	0.02698
C7–C25	0.25278	0.22738
C26–C49	0.05524	0.03747
C50–C64–PN	0.00545	0.0023
C65–C80–PN	0.00183	0.00054
C50–C80–A	0.00256	0.00086
Experimental	Jamaluddin et al. [23]	Jamaluddin et al. fluid A [24]
Characterized	Pedersen et al. [9]	Pedersen et al. [9]
EoS	SRK [27]	PR76 [28]

Table 2. Compositions used for the analysis of methane removal/injection to Case 3.

Component	Original	-80%	-50%	-30%	-15%	10%	20%	50%
N2	0.00480	0.00735	0.00613	0.00552	0.00513	0.00460	0.00442	0.00394
CO2	0.00919	0.01408	0.01174	0.01057	0.00983	0.00881	0.00846	0.00755
C1	0.43391	0.13292	0.27707	0.34919	0.39450	0.45745	0.47911	0.53483
C2	0.1101	0.16864	0.14060	0.12658	0.11776	0.10552	0.10131	0.09047
C3	0.06544	0.10023	0.08357	0.07523	0.07000	0.06272	0.06021	0.05377
iC4	0.00789	0.01209	0.01008	0.00907	0.00844	0.00756	0.00726	0.00648
nC4	0.03787	0.05801	0.04836	0.04354	0.04051	0.03630	0.03485	0.03112
iC5	0.01279	0.01959	0.01633	0.01470	0.01368	0.01226	0.01177	0.01051
nC5	0.02248	0.03443	0.02871	0.02584	0.02405	0.02155	0.02068	0.01847
C6	0.02698	0.04133	0.03446	0.03102	0.02886	0.02586	0.02483	0.02217
C7–C25	0.22738	0.34828	0.29038	0.26141	0.24321	0.21792	0.20922	0.18684
C26–C49	0.03747	0.05739	0.04785	0.04308	0.04008	0.03591	0.03448	0.03079
C50–C64–PN	0.0023	0.00352	0.00294	0.00264	0.00246	0.00220	0.00212	0.00189
C65–C80–PN	0.00054	0.00083	0.00069	0.00062	0.00058	0.00052	0.00050	0.00044
C50–C80–A	0.00086	0.00132	0.00110	0.00099	0.00092	0.00082	0.00079	0.00071

3. Proposed Classification

In this section we will explain the proposed classification, covering all situations encountered. Although we only arrived at such classification after analyzing all behavior variations that will be discussed later, for the sake of clarity in the presentation of results, we first discuss here the different topologies to be considered and assign the corresponding notation.

The majority of phase diagrams calculated presented topologies coincident with those obtained and discussed in the previous work. Therefore, for simplicity and without reasons for a different order, we decided to label those topologies as Types I, II and III respectively. In addition, a new topology was found, combining characteristics of types II and III, and distinguishing from Type II in the same way as Type III distinguishes from Type I, i.e. the upper and lower AOP lines do not meet and therefore there are no DSP's in the phase diagram. This new topology was naturally labeled as Type IV and can be seen in Fig. 2 together with the previous three types.

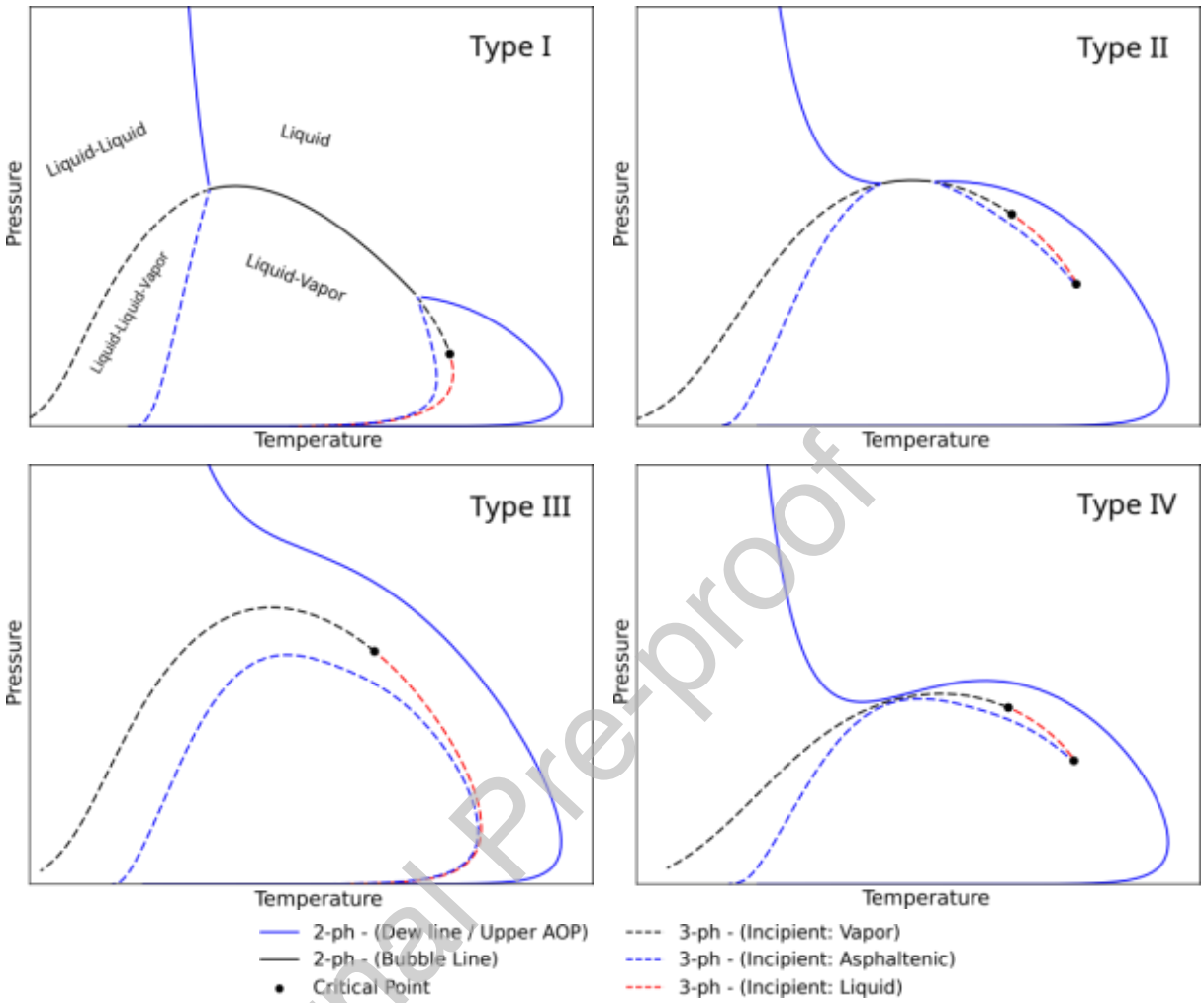

Fig. 2 Proposed classification with four main types of complete phase envelopes for reservoir fluids with asphaltenes. The coloring style of the lines will be the same for the rest of the figures.

Note that the four types result from the combination of possibilities when considering two different aspects of the topology, each of them with two possibilities. The first aspect or question is whether the upper and lower AOP lines, together with the bubble line in between, touch or cross each other. When this happens, which at the same time implies crossings between different two-phase boundaries before discarding unstable segments [17], it gives place to two

All diagrams we have calculated, trying different compositional changes departing from the three case studies, and also others, fall qualitatively in one of these four types. In addition, we have revised different studies in the literature, like those cited in the introduction, and despite the fact that complete diagrams are hard to find, we found nothing that escapes from our classification, based on the partial phase diagrams presented in each work. What we did find in some cases is a different way of arriving at a phase envelope of type II, which challenged our original strategy. Nevertheless, since at first sight the stable phase envelope does not show a qualitative difference with respect to type II, it did not require defining a new type. This situation is therefore discussed in the next section, dedicated to the modifications we had to make to the original algorithmic strategy described in the previous work.

4. Updated Algorithmic Strategy

Now, before presenting and discussing the different sequences of phase envelope variations due to specific compositional changes, we treat here the adaptations that were necessary to make in the general algorithm in order to incorporate some situations not considered before in the original version. In particular, cases were detected where, following the flowchart in Fig. 1, the high-pressure LL line -calculated as the second two-phase boundary- goes down in pressure as an isolated line, instead of passing through a minimum pressure and increase temperature to go around a liquid-vapor region. This led us to incorporate the possibility of a third segment of two-phase boundaries to be calculated in these cases, namely the one starting from a low-T and low-P bubble point, as indicated in Fig. 3. The updated and extended algorithmic strategy is summarized schematically in Fig. 4, as a modification of the flowchart in Fig. 1, already discussed in the introduction.

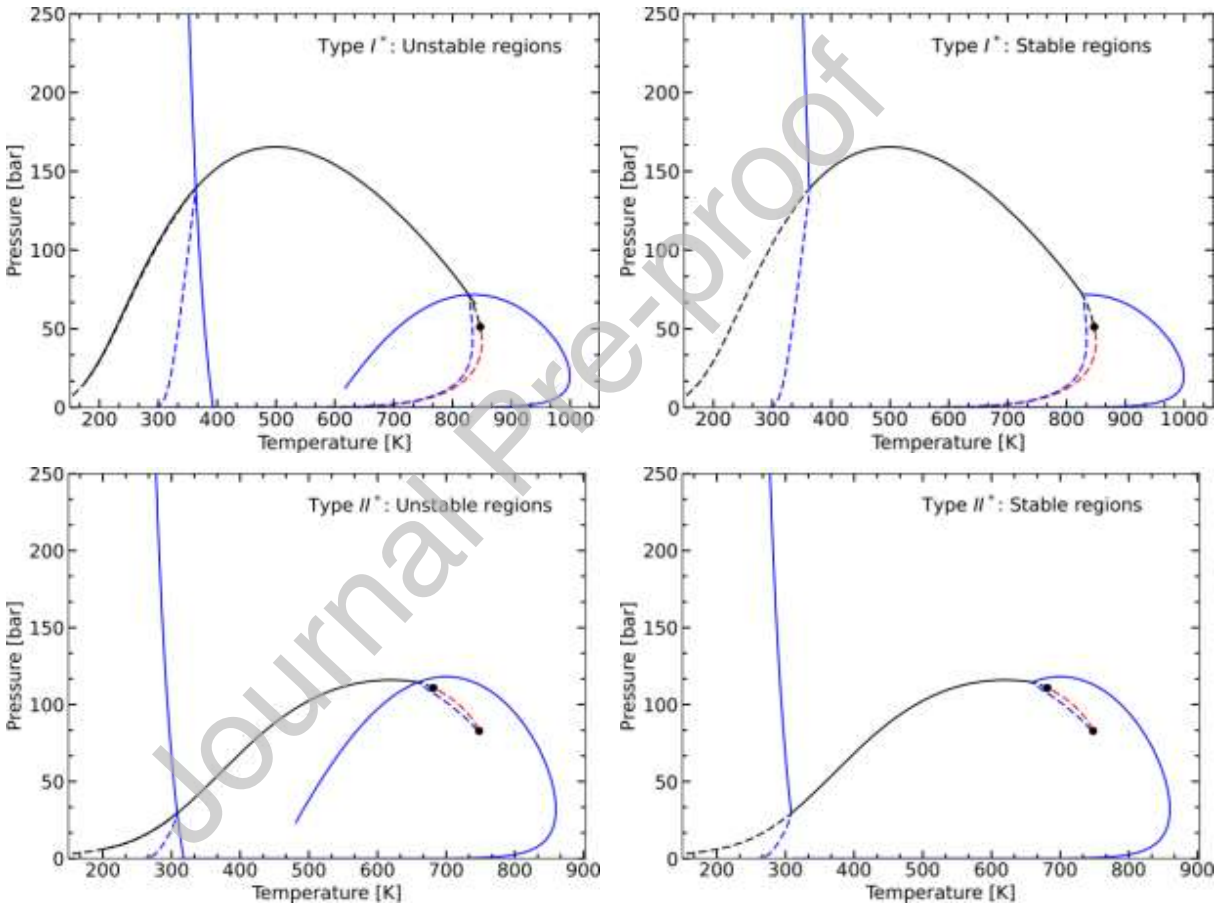

Fig. 3 Examples of phase envelopes corresponding to types I* and II*, including unstable segments on the left side, but only the stable phase diagram on the right.

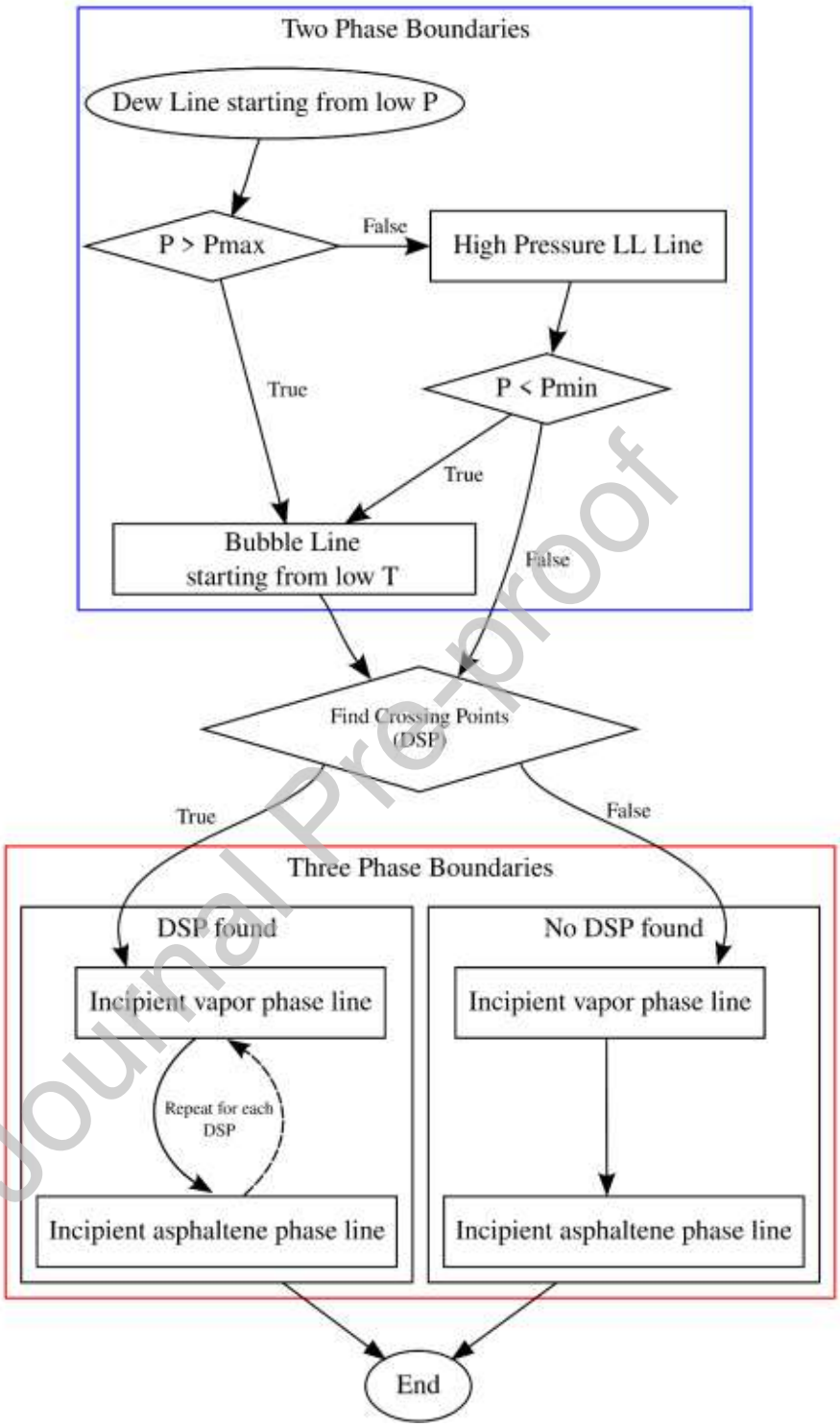

Fig. 4 Flow-chart with the updated algorithmic strategy

5. Compositional effects on phase envelopes and transitions

The effects of compositional changes on phase envelopes were explored based on the removal/injection of different compounds or fractions, as explained above in the Methodology section. Moreover, a special focus was put in identifying transitions between the different types of phase behavior covered in the proposed classification. For example, Fig. 5 shows the effect of the methane content on the predicted phase diagram for variations of Case 3 (see Table 2 for detailed compositions). It is clearly seen for this case study that a higher content of methane induces or favors the precipitation of asphaltenes, increasing the temperatures and pressures of the upper AOP line and also the extension of three-phase regions. A more detailed animation of this transition can be found on the suplementary material.

This, which is consistent with previous studies dealing with the effect of gas injection on asphaltene precipitation behavior, was also observed in our study for variations of Cases 1 and 2, as shown for the latter in Fig. 6. The evolutions of phase diagrams observed in Figs. 5 and 6 are similar, with the only important difference being that in the first one the observed transition is I → III, while in the second we have II → IV.

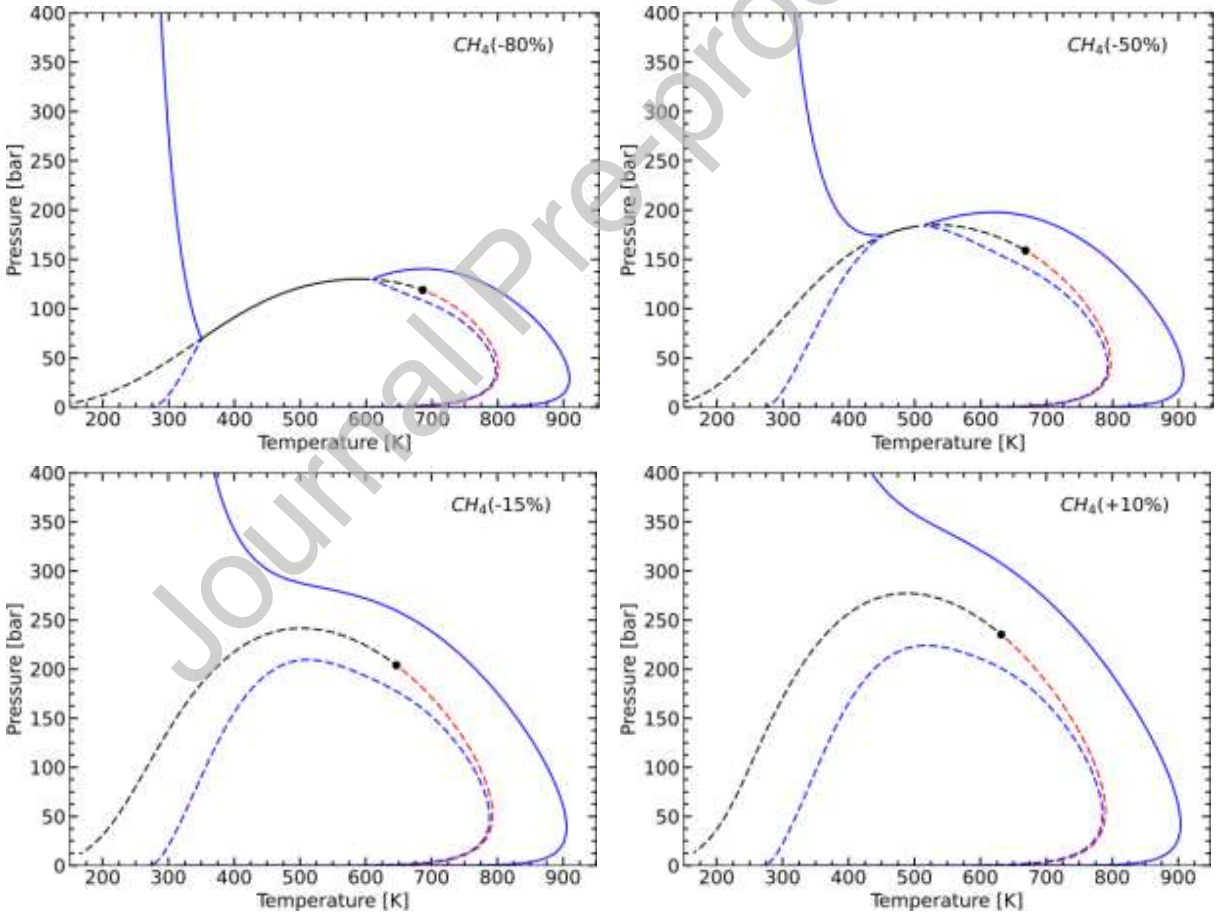

Fig. 5 Effect of methane content on predicted phase diagram for variations of Case 3. A transition from type I to type III is observed.

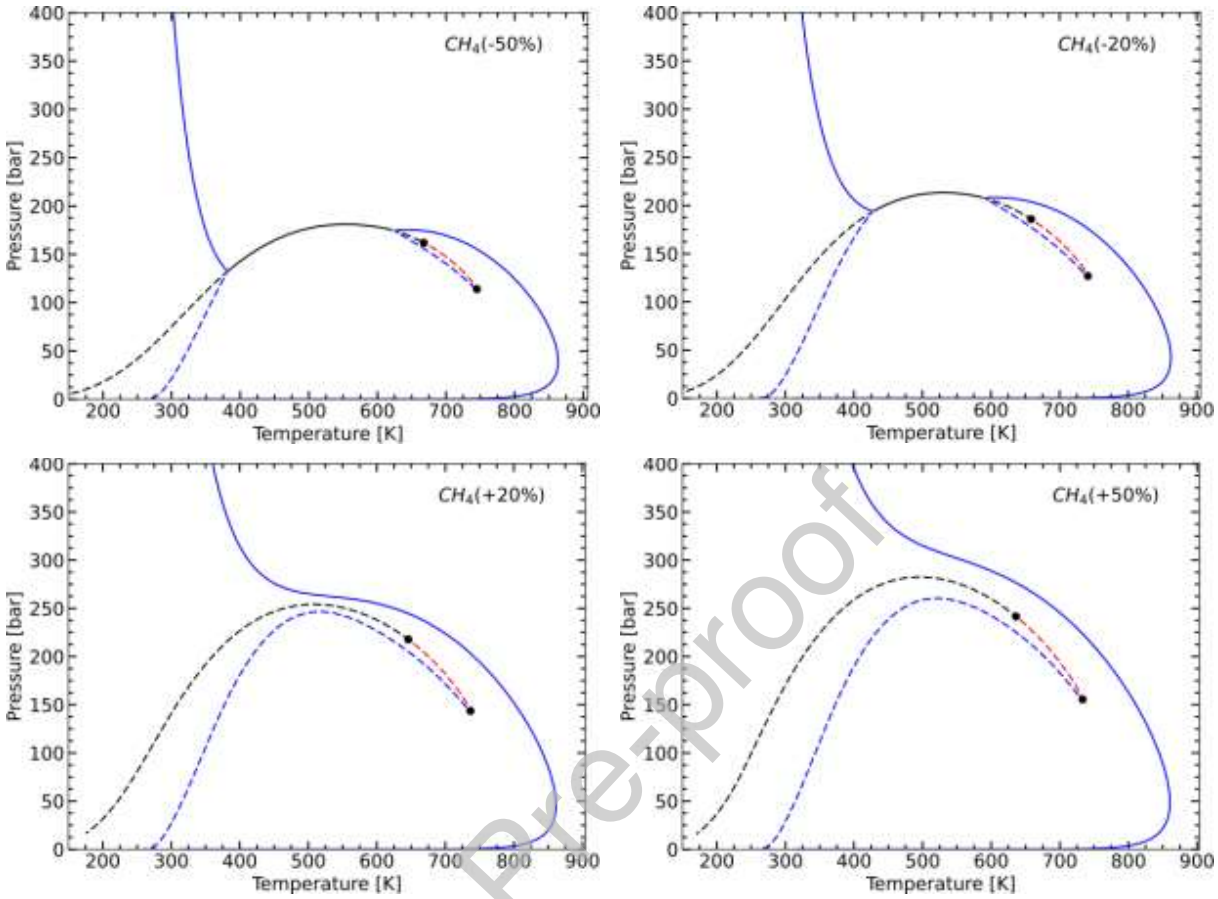

Fig. 6 Effect of methane content on predicted phase diagram for variations of Case 2. A transition from type II to type IV is observed.

Moreover, equivalent evolutions can be observed based on the injection or removal of other gasses, for the same cases. The effects of CO_2 and H_2S are illustrated in Figs. 7 and 8 for Case 2, a detailed animation of the effects of CO_2 can be found in the supplementary material. Note that the effect of H_2S on the AOP lines is softer in comparison to those of methane and CO_2. However, when analyzing this type of figures it is important to keep in mind that the informed variations are relative to the original content of the compound in the fluid studied. Then, for example, +600% in Fig. 8 means increasing the H_2S mole fraction from 0.0322 to 0.1889, while +50% in Fig. 6 implies going from 0.2736 to 0.3610 in the mole fraction of methane. All detailed compositions are provided in the supplementary material. We must also remark that the effects of H_2S content observed here should be taken with caution, since the model defined by Pedersen et al. [9] for this fluid, and adopted here, does not account for association effects that could be important between H_2S and asphaltenes and even a null k_{ij} was used. A brief analysis on the impact of the k_{ij} parameter on the type of phase diagram transition is presented in Appendix D.

Nevertheless, despite this particular case of H_2S for which we are not aware of any experimental study, the effects of non-associating gases, mainly methane and CO_2, are already well known in the literature, both from experimental and modeling studies. Indeed, the type of transition observed here (I to III or II to IV) is the one shown for example by Panuganti et al. [11] in their Fig. 7 or in the work of Arya et al. [14]

in their Fig. 5, although in a more restricted and partial view, as a consequence of varying gas content in the oil.

Moreover, Fig. 9 shows a crossover point among the upper AOP lines with varying contents of CO_2 for Case 2, similar to what was reported by Gonzalez et al. (2008) [10] and Mohebbinia et al. (2017) [16] using PC-SAFT. It is interesting to see that the same qualitative effect is obtained here with the SRK EoS. Similarly, but more pronounced and for not so high pressures, such crossover behavior was also found as consequence of injecting H_2S in Case 2, as depicted in Fig. 10. This effect, indicating that H_2S could favor asphaltene stabilization in solution in the lower temperature range, would require experimental confirmation. Especially in view that, as already expressed above, the modelling or parameterization of this compound and its interactions might not be the appropriate one in this example.

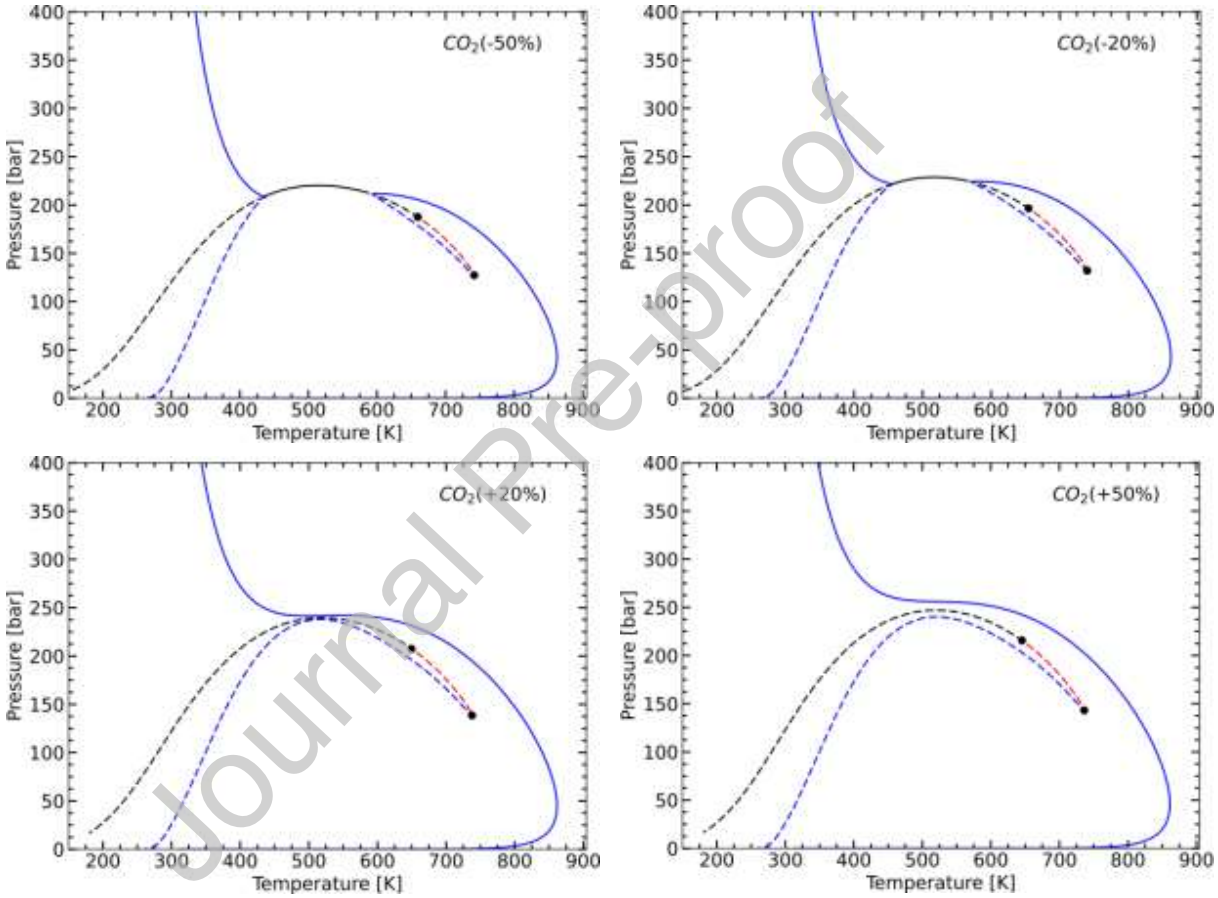

Fig. 7 Effect of CO_2 content on predicted phase diagram for variations of Case 2. A transition from type II to type IV is observed.

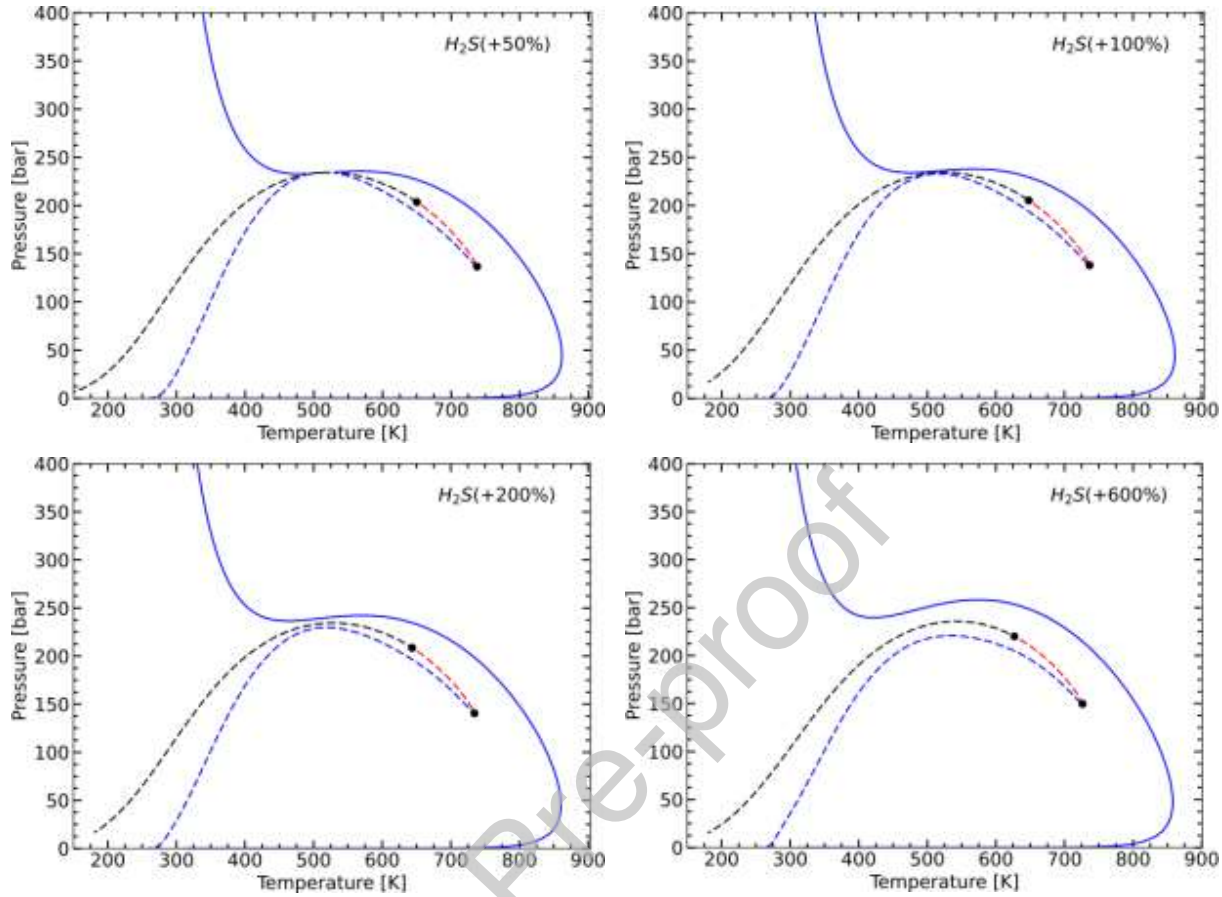

Fig. 8 Effect of H_2S content on predicted phase diagram for variations of Case 2. A transition from type II to type IV is observed.

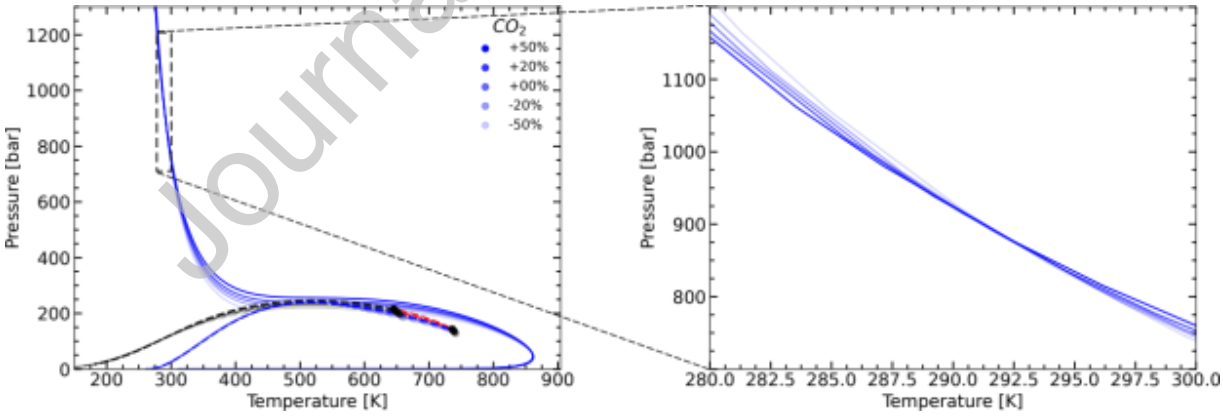

Fig. 9 Crossover in the upper AOP curve, as an effect of CO_2 content variations in Case 2. Increase in the color saturation refers an increase in the CO_2 concentration.

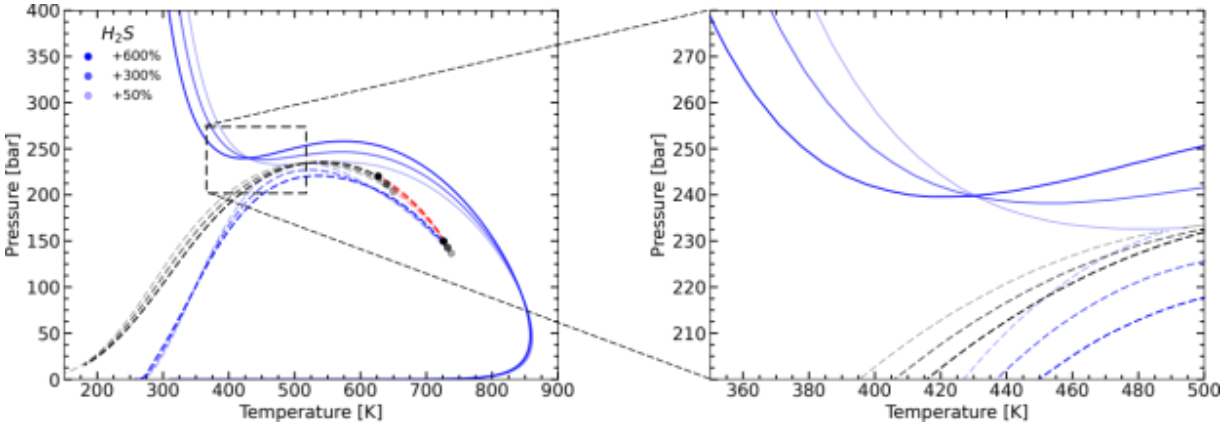

Fig. 10 Crossover in the upper AOP curve, as an effect of H_2S content variations in Case 2. Increase in the color saturation refers an increase in the H_2S concentration.

Figs. 11 and 12 show the effect of asphaltene content in Cases 2 and 3 respectively. In both cases, as expected, a higher content of asphaltenes shifts the upper AOP curve to higher temperatures and pressures, favoring asphaltenes precipitation.

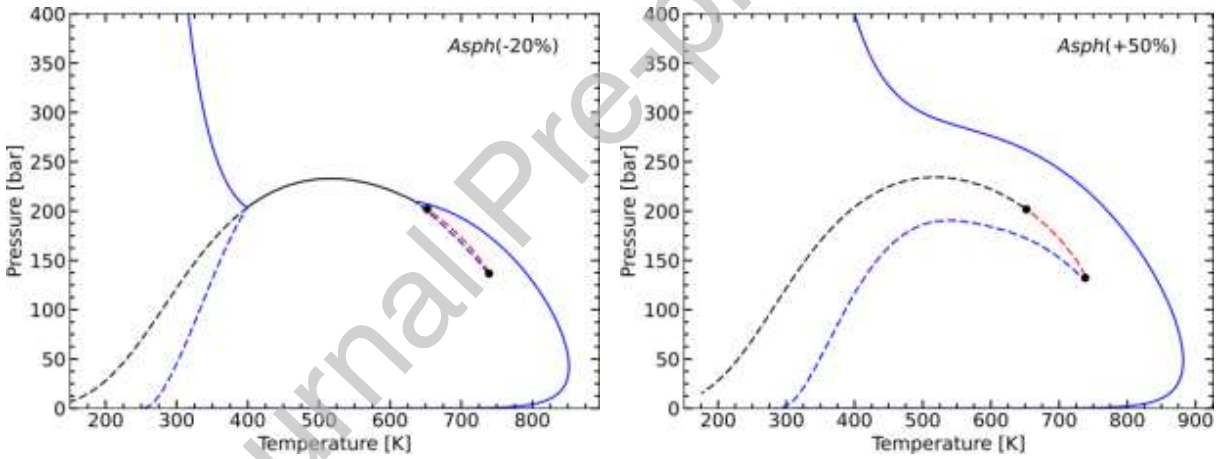

Fig. 11 Effect of asphaltene content on predicted phase diagram for variations of Case 2. A transition from type II to type IV is observed.

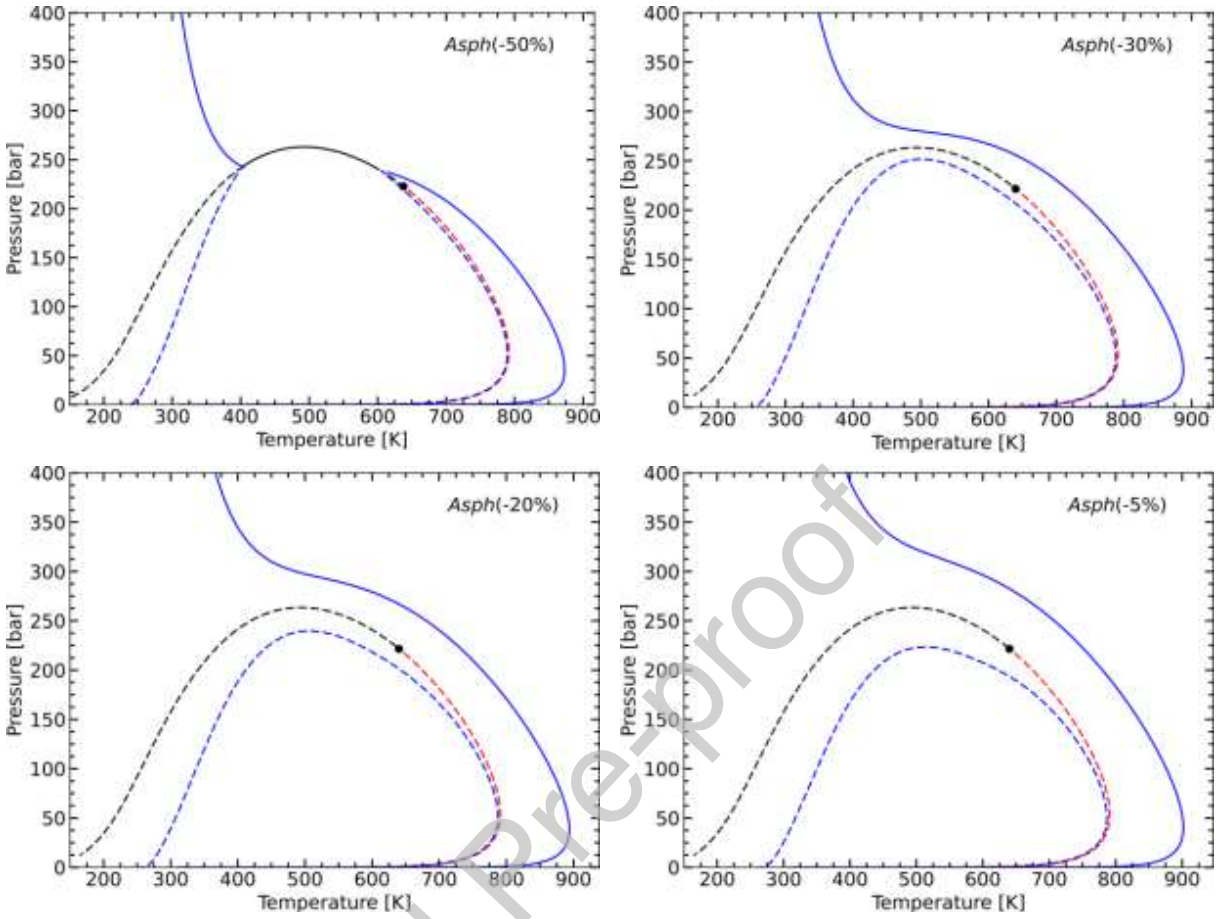

Fig. 12 Effect of asphaltene content on predicted phase diagram for variations of Case 3. A transition from type I to type III is observed.

What is not typically analyzed is the effect of other intermediate compounds or fractions. Fig. 13 shows how the phase diagram is modified for Case 2 when fractions including from C5 to C25 are removed or injected, while equivalent effects were observed for Cases 1 and 3. Contrary to what was found for either gasses or asphaltenes, it is clearly seen that increasing the content of intermediate fractions -and therefore decreasing both asphaltenes and the most volatile fractions- improves the miscibility of the system and stabilizes asphaltenes in solution, decreasing AOP temperatures and/or pressures. This reduction of the molecular asymmetry in the composition leads to transitions from type IV to II in this case, or analogously from III to I, which are opposite to the ones found before, as a consequence of injecting gasses or asphaltenes.

Up to this point, we can say that the evolution of the topological behavior of a specific system was evaluated from the point of view of the thermodynamic models, both in terms of the injection of light gasses (CH_4, CO_2, and H_2S) and by modifying the concentration of pseudo-compounds or asphaltenes. It was observed that increasing/decreasing the concentration of any of these, always leads to similar results, namely, an increase/decrease in the pressure and temperature of the AOP-line, respectively. As a consequence of the displacement of the AOP-line, the three-phase region is modified, giving rise to a topological transition, as observed in Figures 5 to 8. In this sense, we can analyze how modifying the concentration of a compound in the system leads to a transition between two different topologies. There

are several aspects that can influence such changes, but we believe there are two fundamental ones: the volatility and polarity of the compounds injected/removed, and how they modify the symmetry/asymmetry of the system, stabilizing/destabilizing the asphaltene phase. Both CH_4 and CO_2 are non-polar components with high volatility, so the incorporation of such components increases the asymmetry of the system, in particular with respect to asphaltenes, which are characterized by having higher polarity. It is expected that the asphaltenic phase destabilizes with the increase in the concentration of these two components.

On the other hand, we have in H_2S a volatile compound, but unlike CH_4 and CO_2, it is highly polar. Its volatility contributes to elevating the AOP-line (Fig 8). However, this compound has a greater affinity with asphaltenes than CH_4 and CO_2, which means that large concentrations of H_2S are required to substantially modify the AOP-line and achieve a topological transition. Next, we have the effect of modifying the concentration of asphaltenes. Naturally, an increase in their concentration in a given fluid will result in an early appearance of the asphaltene phase, indicating an increase in the asymmetry of the system. Regarding the pseudo-compound C5-C25, it is observed that its removal shifts the AOP line upwards, favoring the appearance of the asphaltenic phase. As the concentration of C5-C25 increases, diluting at the same time both asphaltenes and the lighter components, the AOP line shifts to lower pressures and temperatures. This suggests that the miscibility increases as the system's asymmetry decreases, when injecting intermediate fractions.

Table 3 summarizes all compositional effects found in this study, in particular on AOPs, bubble line pressures and extension of three-phase region. Figs. showing the effects of C5-6, as well as other not shown here so far, are included as supplementary material. The fraction C5-6 can be considered as light-intermediate, and its effects are in general similar to those of the larger fraction C5-25 but softer. It is important to mention that the effects computed with the thermodynamic models in this study are consistent with experimental observations. Appendix B correlates the results obtained in this study with the experimental observations found in the literature.

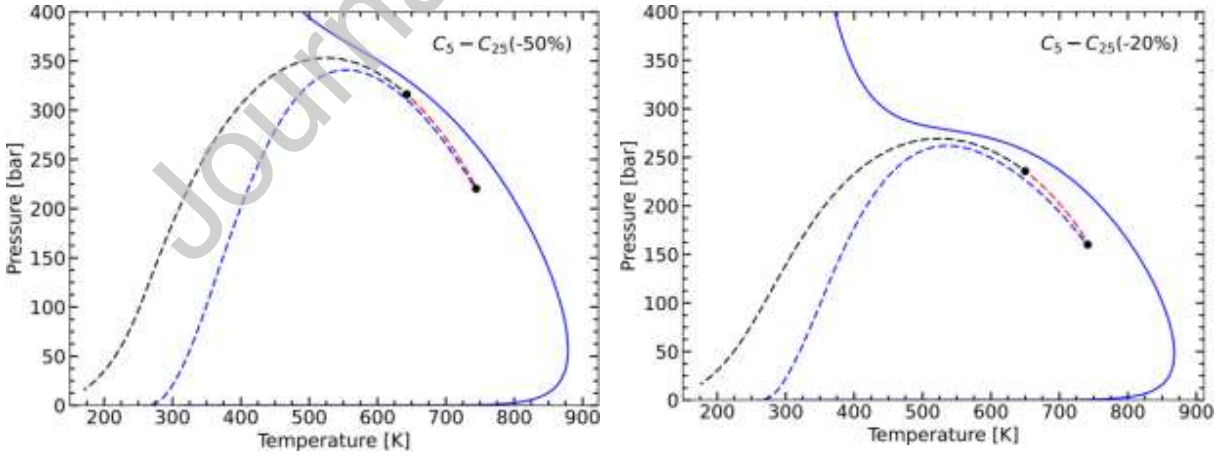

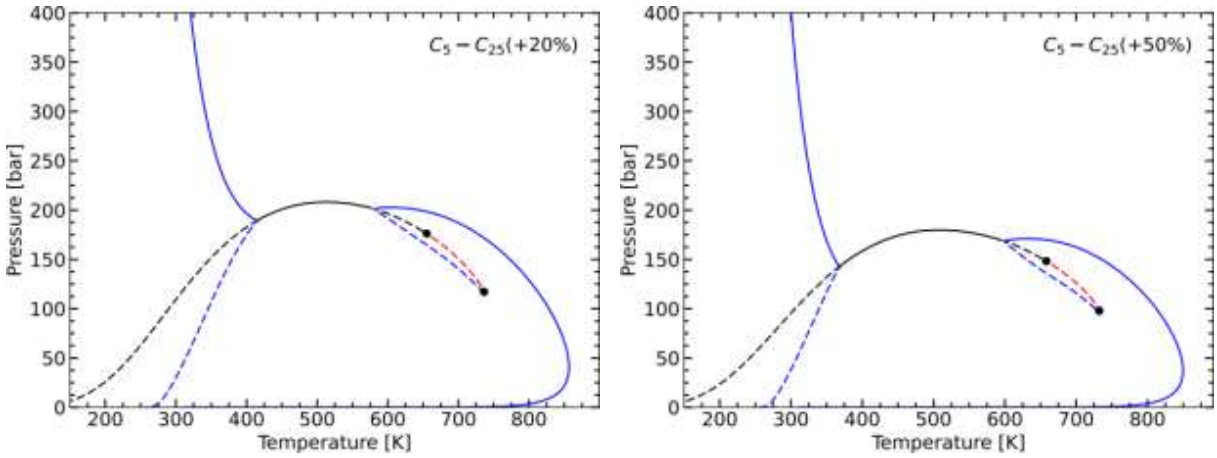

Fig. 13 Effect of intermediate fractions content on predicted phase diagram for variations of Case 2. A transition from type IV to type II is observed.

Table 3. Qualitative effects on AOP, bubble line pressures and extension of three-phase region, caused by the increment in concentration of each studied component (a decrease would cause the opposite effect).

	CO_2	CH_4	H_2S^*	$C_{5\text{-}6}$	$C_{5\text{-}25}$	Asphaltenes
AOP	Increase	Strong Increase	Increase	No change	Strong decrease	Strong increase
Bubble Line	Increase	Strong Increase	No change	Decrease	Slight decrease	No change
3-ph region	Slight Increase in whole area	Increase in pressure and whole area	Slight increase in whole area	Slight decrease	Slight decrease	Increase in whole area

*: H_2S was only studied in case 2

In terms of transitions, it is important to highlight that only transitions between types I and III or between types II and IV have been observed so far in this work. Transitions like I → II or III → IV would imply the appearance of a critical point in the higher temperature part of the three-phase boundary, closing the three-phase region. We did search for that kind of transition, trying different compositional variations apart from those exposed and discussed above, without success, with one particular exception to be explained below. Based on that, and examining in detail the characterizations and compositions of the fluids in the three case studies considered, we arrived to the hypothesis that in general types I and III can be predicted, quite independently of the composition, when the asphaltene pseudo-component and the second heaviest (non-asphaltenic) compound are sufficiently different in terms of parameters, which is the situation with cases 1 and 3 studied here. Instead, that difference is not that important in Case 2, which allows reaching the second critical point which is characteristic of types II and IV. In this view, which so far requires further analysis and confirmation, types II and IV could be considered more realistic for typical real reservoir fluids, where there is a compositional continuum in which asphaltenes are just the

extreme tail of a distribution[29]. On the other hand, types I and III would be the consequence of model limitations due to the compositional discretization or grouping adopted for the characterization of the fluid (lumping strategy), unless real compositional gaps are present in the fluid. For example, types I or III could be expected experimentally for synthetic oils formed by dissolving some previously isolated asphaltenes in a light oil or solvent mixture. To confirm the hypothesis, the effect of the lumping adopted, with more or less pseudo compounds to represent the heavier fractions, needs to be analyzed.

But before, as expressed above, there was an exception involving the transition III → IV, obtained by a specific compositional modification of Case 3, which consisted of removing the heaviest non-asphaltenic pseudo compound, i.e. C65–C80–PN. The occurrence of this transition, exposed in Fig. 14, might in principle appear as contradictory with the hypothesis and interpretation developed above, since -in modelling terms- that type of pseudo compound is usually something intermediate between asphaltenes and the lighter compounds, so its removing should not favor the criticality implied in this transition, but just the opposite. However, this is not the case. Quite strangely in the parameterization of this fluid in comparison to Cases 1, 2 and others, this heaviest non-asphaltenic pseudo-compound (C65–C80–PN) has clearly the largest values of both a_c and b -and therefore m value- for such range of carbon numbers (see the parameter Tables in Appendix A). In other words, the asphaltene pseudo-compound can be seen as C50–C64–PN C65–C80–PN. That explains why removing the latter allows to close the three-phase region with the implied criticality between the two liquid phases, leading to an envelope of type IV, while that was not possible with the original composition, due to the presence of this extremely heavy non-asphaltenic pseudo compound that could be interpreted as very heavy paraffins. It must be noticed here that part of the anomaly in this pseudo compound, namely the low value of 0.182 for the acentric factor, has its roots in the correlation for *m* used by Pedersen et al. [9], which has a quadratic dependence with molecular weight, presenting a maximum around 550, i.e. carbon numbers in the range of 40.

Now, having explained the exceptionality of Case 3 and the very particular III → IV transition obtained, this case offers us the opportunity to test the effect of the lumping, in particular the number of pseudo compounds, in order to see if the results are consistent with the hypothesis expressed above, and to do it in two different ways: with the original correlation for *m* / acentric factor and with an alternative correlation without a maximum, allowing for a better continuity towards asphaltenes. Fig. 15 presents the predicted complete phase envelopes for the Case 3 fluid, with 1, 2, 4, and 8 non-asphaltenic pseudo compounds to represent the C7+ fraction, maintaining the rest of the Pedersen methodology unaltered, including the *m* values correlation. The details of each lumping, with the corresponding parameters, can be found in Appendix E, Tables E1 to E4, noting that the grouping into four pseudo compounds + asphaltenes corresponds to the original Case 3 as considered in Tables 1 and A5.

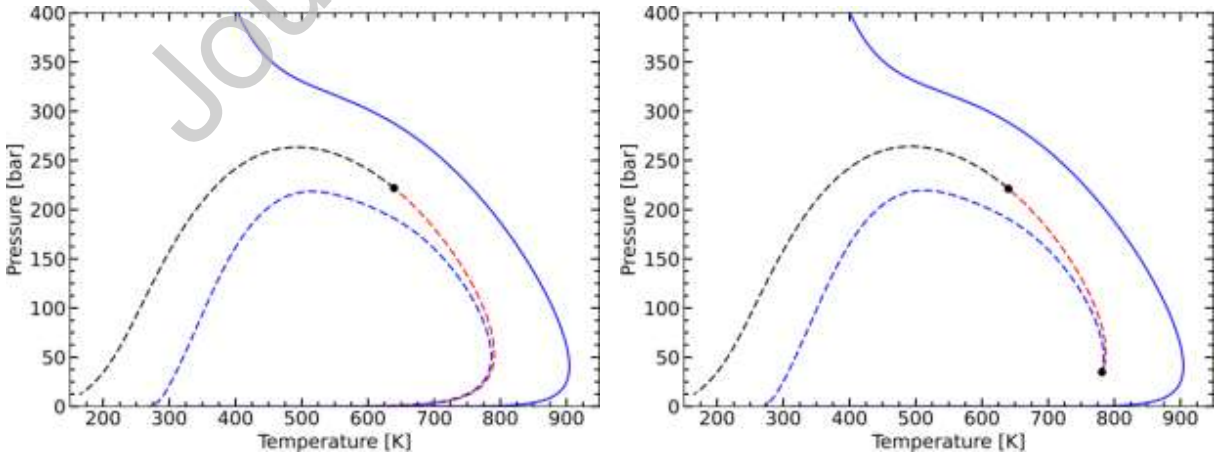

Fig. 14 A transition from type III (left) to type IV (right), encountered in the very particular Case 3, by removing the last non-asphaltenic pseudo-compound C65–C80–PN.

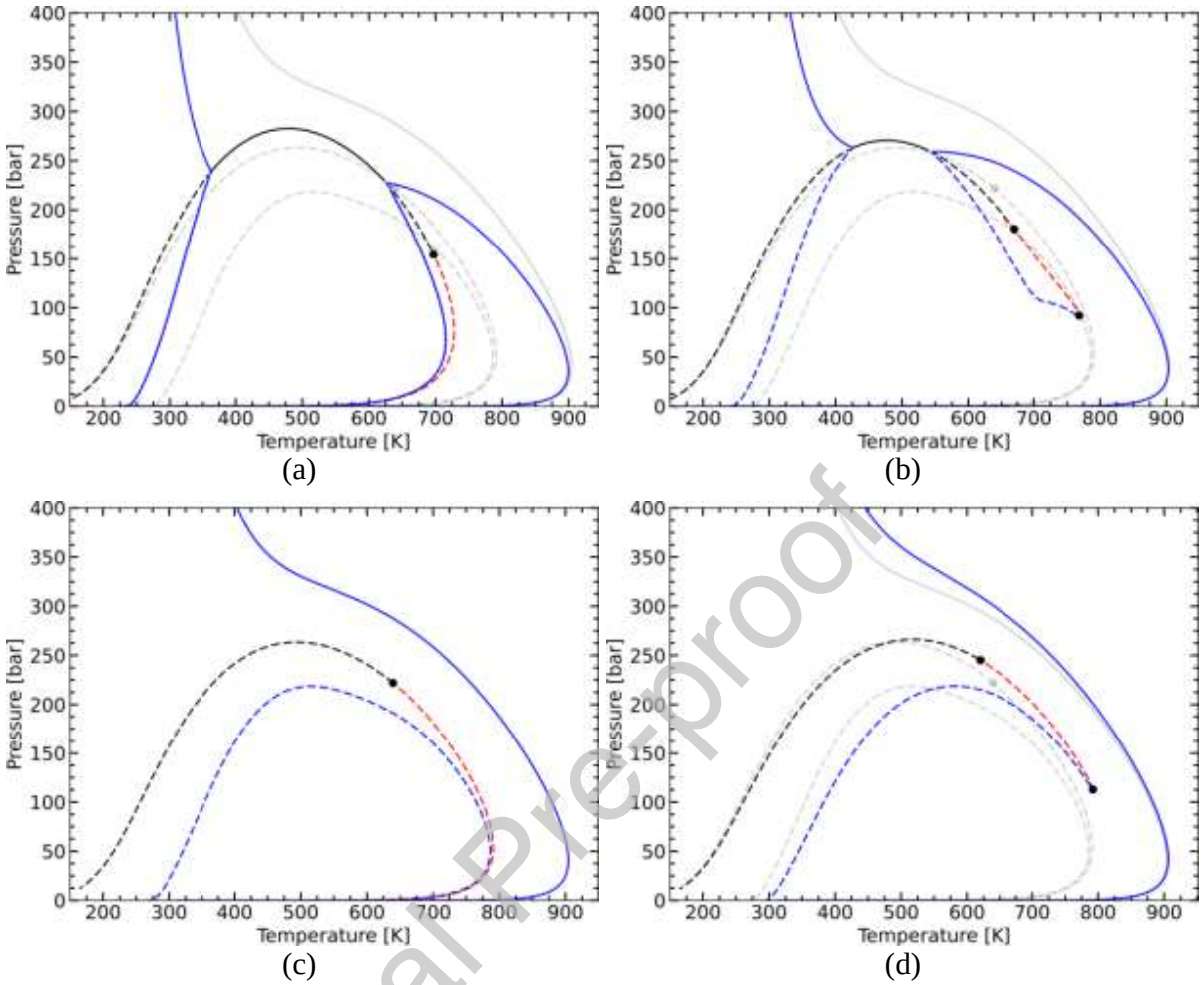

Fig. 15 Impact from lumping strategy for the C7+ fraction in Case 3 on the predicted type of phase diagram. (a): 1 pseudo-component + asphaltenes – type I, (b): 2 pseudo-components + asphaltenes – type II, (c): 4 pseudo-components + asphaltenes – type III, and (d): 8 pseudo-components + asphaltenes – type IV.

Remarkably, not only a clear effect of the lumping strategy can be seen in Fig. 15, but also the four types included in the proposed classification have been obtained for the same fluid, just by varying the number of pseudo compounds in which the C7+ distribution is grouped. It should be noted, however, that this specific evolution I → II → III → IV is not something to be naturally anticipated for this or other fluids. Instead, in our view, it was an unexpected consequence of the lumping effect, in combination with the particular parameterization of the fluid and the Pedersen correlation for *m*, already mentioned. Still, two out of the three transitions confirm the expected effect that a finer lumping, i.e. more pseudo compounds, should favor the mixing between asphaltenes an the heaviest non-asphaltenic pseudo-compound and therefore promote the transitions from types I/III to types II/IV. Then, when replacing the original correlation for *m* by an alternative exponential function which is numerically similar in the low molecular weight range but without presenting a maximum, the resulting evolution is I → II → IV → IV, also for 1, 2, 4 and 8 non-asphaltenic pseudo compounds and the same carbon number ranges (see Tables E1 to E4) as shown in Fig. E1. This is completely consistent with the ideas expressed above.

6. Conclusions

Based on an algorithm presented in a previous publication it was possible to explore the effects of different compositional changes on the complete phase diagrams predicted for reservoir fluids with asphaltenes, as modelled with equations of state. This exploration led to the finding of a new topology and also variations for previously reported types. Moreover, a classification of four types plus variations has been proposed. The main features defining each type of behavior are the existence of DSP and the presence of a second critical point along the three-phase boundary, which defines the extension of the three-phase region. The original algorithm has been updated in order to consider cases where an isolated liquid-liquid saturation line crosses a low-temperature bubble line.

Transitions between types I-III, as well as between II-IV, have been identified as the result of distinct compositional changes, e.g.: gas injection. Other types of transitions (e.g.: I<->II or III<->IV) can be the consequence of modeling decisions, like the criteria used to define a pseudo-compound (lumping), the pure compound parameters assigned, and the interaction parameters (kij parameter) defined for the complete system. Their (nearly) nonoccurrence as a result of compositional changes allowed to formulate hypotheses regarding what type of real systems or what type of limitations in the characterization of reservoir fluids could be responsible for phase diagrams of types I or III.

In summary, as it has been demonstrated in this work, the updated algorithm for direct computation of complete phase envelopes can be very useful in the study of the effects of compositional changes and characterization methodologies on the predicted high-pressure phase behavior of asphaltenes in reservoir fluids from equations of state. The option to perform this type of studies by scanning the T-P space with a flash algorithm would be much more complicated, tedious and time consuming. Moreover, the proposed classification of phase envelope types should be useful to researchers or professionals working in the area, either to design or guide experiments, to better interpret and integrate experimental data as well as model predictions, and also to consider possible extrapolations to other ranges of temperature and pressure, among other possibilities. In relation to composition effects, the results presented and discussed in this work can help to anticipate how the phase diagram can change and what transitions can be expected in processes like gas injection or mixing of fluids.

It is important to remark that the updated algorithm presented in this work, as well as the proposed classification and transitions discussed, cover reservoir fluids with asphaltenes. While the presence of small quantities of CO_2, H_2S or even water or other polar compounds may not alter qualitatively the possibilities, one has to be aware that above certain concentration levels, which will depend on the case, these compounds can induce the formation of other three-phase regions, leading to different topologies and in some cases even the occurrence of four-phase regions.

Acknowledgements

The authors want to thank Oscar Ivan Theran Becerra (IPQA-CONICET) for assistance with the computations for delumping and re-lumping the heavy pseudo-components in Case 3.

Financial support from FONCyT (PICT 2021-0008) and SECyT-UNC is acknowledged. G.O.P. and M.C.D. are researchers from Consejo Nacional de Investigaciones Científicas y Técnicas (CONICET). F.E.B. is a research fellow of CONICET.

References

[1] F.M. Vargas, M. Tavakkoli, Asphaltene Deposition: Fundamentals, Prediction, Prevention, and Remediation, 1st ed., CRC, 2018. https://doi.org/https://doi.org/10.1201/9781315268866.

[2] J. Beck, W.Y. Svrcek, H.W. Yarranton, Hysteresis in asphaltene precipitation and redissolution, Energy and Fuels. 19 (2005) 944–947. https://doi.org/10.1021/ef049707n.

[3] S. Peramanu, C. Singh, M. Agrawala, H.W. Yarranton, Investigation on the reversibility of asphaltene precipitation, Energy and Fuels. 15 (2001) 910–917. https://doi.org/10.1021/ef010002k.

[4] A. Hammami, C.H. Phelps, T. Monger-McClure, T.M. Little, Asphaltene precipitation from live oils: An experimental investigation of onset conditions and reversibility, Energy and Fuels. 14 (2000) 14–18. https://doi.org/10.1021/ef990104z.

[5] A. Abedini, S. Ashoori, F. Torabi, Y. Saki, N. Dinarvand, Mechanism of the reversibility of asphaltene precipitation in crude oil, J. Pet. Sci. Eng. 78 (2011) 316–320. https://doi.org/10.1016/j.petrol.2011.07.010.

[6] F. Width, Reversibility of Asphaltene Aggregation Quantitative Evaluation Saber Mohammadi , † Fariborz Rashidi , * , ‡ Sayed Ali, 4105 (2018) 6–7.

[7] P. Agrawal, F.F. Schoeggl, M.A. Satyro, S.D. Taylor, H.W. Yarranton, Measurement and modeling of the phase behavior of solvent diluted bitumens, Fluid Phase Equilib. 334 (2012) 51–64. https://doi.org/10.1016/j.fluid.2012.07.025.

[8] G.M. Kontogeorgis, G.K. Folas, Industrial Applications Thermodynamic Models for Industrial Applications From Classical and Advanced, 2010.

[9] K. Pedersen, P. Christensen, J. Shaikh, Phase Behavior of Petroleum Reservoir Fluids, Second, CRC/Taylor & Francis, 2015.

[10] D.L. Gonzalez, F.M. Vargas, G.J. Hirasaki, W.G. Chapman, Modeling study of CO2-induced asphaltene precipitation, Energy and Fuels. 22 (2008) 757–762. https://doi.org/10.1021/ef700369u.

[11] S.R. Panuganti, F.M. Vargas, D.L. Gonzalez, A.S. Kurup, W.G. Chapman, PC-SAFT characterization of crude oils and modeling of asphaltene phase behavior, Fuel. 93 (2012) 658–669. https://doi.org/10.1016/j.fuel.2011.09.028.

[12] A. Arya, N. von Solms, G.M. Kontogeorgis, Determination of asphaltene onset conditions using the cubic plus association equation of state, Fluid Phase Equilib. 400 (2015) 8–19. https://doi.org/10.1016/j.fluid.2015.04.032.

[13] A. Arya, N. Von Solms, G.M. Kontogeorgis, Investigation of the Gas Injection Effect on Asphaltene Onset Precipitation Using the Cubic-Plus-Association Equation of State, Energy and Fuels. 30 (2016) 3560–3574. https://doi.org/10.1021/acs.energyfuels.5b01874.

[14] A. Arya, X. Liang, N. Von Solms, G.M. Kontogeorgis, Modeling of Asphaltene Onset Precipitation Conditions with Cubic Plus Association (CPA) and Perturbed Chain Statistical Associating Fluid Theory (PC-SAFT) Equations of State, Energy and Fuels. 30 (2016) 6835–6852. https://doi.org/10.1021/acs.energyfuels.6b00674.

[15] A. Arya, X. Liang, N. Von Solms, G.M. Kontogeorgis, Prediction of Gas Injection Effect on Asphaltene Precipitation Onset Using the Cubic and Cubic-Plus-Association Equations of State, Energy and Fuels. 31 (2017) 3313–3328. https://doi.org/10.1021/acs.energyfuels.6b03328.

[16] S. Mohebbinia, K. Sepehrnoori, R.T. Johns, A. Kazemi Nia Korrani, Simulation of asphaltene precipitation during gas injection using PC-SAFT EOS, J. Pet. Sci. Eng. 158 (2017) 693–706. https://doi.org/10.1016/j.petrol.2017.09.008.

[17] M. Cismondi, Phase Envelopes for Reservoir Fluids with Asphaltene Onset Lines: An Integral Computation Strategy for Complex Combinations of Two- and Three-Phase Behaviors, Energy and Fuels. 32 (2018) 2742–2748. https://doi.org/10.1021/acs.energyfuels.7b02790.

[18] M. Michelsen, J. Mollerup, Thermodynamic Models: Fundamentals and Computational Aspects, 2007. http://www.tie-tech.com/products/publications/more.php?id=32_0_1_0_M13.

[19] M. Cismondi, M.L. Michelsen, Global phase equilibrium calculations: Critical lines, critical end points and liquid-liquid-vapour equilibrium in binary mixtures, J. Supercrit. Fluids. 39 (2007). https://doi.org/10.1016/j.supflu.2006.03.011.

[20] M. Cismondi, M. Michelsen, Automated calculation of complete Pxy and Txy diagrams for binary systems, Fluid Phase Equilib. 259 (2007). https://doi.org/10.1016/j.fluid.2007.07.019.

[21] M. Cismondi, M.L. Michelsen, M.S. Zabaloy, Automated generation of phase diagrams for binary systems with azeotropic behavior, Ind. Eng. Chem. Res. 47 (2008). https://doi.org/10.1021/ie8002914.

[22] N.E. Burke, R.E. Hobbs, S.F. Kashou, Measurement and modeling of asphaltene precipitation, JPT, J. Pet. Technol. 42 (1990) 1440–1446. https://doi.org/10.2118/18273-PA.

[23] A.K.M. Jamaluddin, N. Joshi, F. Iwere, O. Gurpinar, An Investigation of Asphaltene Instability under Nitrogen Injection, Proc. SPE Int. Pet. Conf. Exhib. Mex. (2002) 427–436. https://doi.org/10.2118/74393-ms.

[24] and M. Jamaluddin, A.K.M., Joshi, N., Joseph, M.T., D'Cruz, D., Ross, B., Creek, J., Kabir, C.S., J.D., Laboratory techniques to define the asphaltene precipitation envelope, in: Pet. Soc. Can. Int. Pet. Conf., 2000.

[25] K. Gonzalez, H. Nasrabadi, M. Barrufet, Modeling asphaltene precipitation in a compositional reservoir simulator using three-phase equilibrium, J. Pet. Sci. Eng. 154 (2017) 602–611. https://doi.org/10.1016/j.petrol.2016.09.010.

[26] D.B. Robinson, D.Y. Peng, The Characterization of the Heptanes and Heavier Fractions for the GPA Peng-Robinson Programs, Gas Processors Association, 1978.

[27] G. Soave, Equilibrium constants from a modified Redlich-Kwong equation of state, Chem. Eng. Sci. 27 (1972) 1197–1203. https://doi.org/10.1016/0009-2509(72)80096-4.

[28] D.Y. Peng, D.B. Robinson, A New Two-Constant Equation of State, Ind. Eng. Chem. Fundam. 15 (1976) 59–64. https://doi.org/10.1021/i160057a011.

[29] M.E. Moir, Asphaltenes, What Art Thou?: Asphaltenes and the Boduszynski Continuum, ACS Symp. Ser. 1282 (2018) 3–24. https://doi.org/10.1021/bk-2018-1282.ch001.

[30] M.I.L. Abutaqiya, C.J. Sisco, Y. Khemka, M.A. Safa, E.F. Ghloum, A.M. Rashed, R. Gharbi, S. Santhanagopalan, M. Al-Qahtani, E. Al-Kandari, F.M. Vargas, Accurate Modeling of Asphaltene Onset Pressure in Crude Oils under Gas Injection Using Peng-Robinson Equation of State, Energy and Fuels. 34 (2020) 4055–4070. https://doi.org/10.1021/acs.energyfuels.9b04030.

Appendix A: Parameters of the reference fluids in the three case studies

Case 1:

Table A1: Pure compound parameters [24]. PR78-EOS [25]

Component	Tc(K)	Pc(bar)	w	ac(bar*L2/mol2)	b(L/mol)	m
CO2	304.039	73.79	0.225	3.96	0.027	0.708
C1-N	189.428	45.83	0.009	2.475	0.027	0.388
C2-C	339.872	45.41	0.127	8.041	0.048	0.566
C4	419.817	37.54	0.188	14.84	0.072	0.655
C5	465.094	33.8	0.24	20.229	0.089	0.729
C6	507.317	32.9	0.275	24.727	0.1	0.778
C7+n	860.372	12.46	1.022	187.786	0.447	1.743
Asph	1424.81	12.29	1.441	522.126	0.75	2.228

Table A2: k_{ij} interaction parameters [24] for PR-EOS [25]. The interaction parameters not included in the table correspond to a zero value for:

	C1-N	C2-C	C4	C5
C7+n	0.053	0	0	0
Asph	0.135	0.135	0.135	0.135

Case 2:

Table A3: Pure compound parameters [8]. SRK-EOS[26]

Component	Tc(K)	Pc(bar)	w	ac(bar*L2/mol2)	b(L/mol)	m
N2	126.2	33.94	0.04	1.387	0.027	0.543
CO2	304.2	73.76	0.225	3.708	0.03	0.825
H2S	373.25	89.37	0.1	4.607	0.03	0.636
C1	190.6	46	0.008	2.334	0.03	0.493
C2	305.4	48.84	0.098	5.644	0.045	0.633
C3	369.8	42.46	0.152	9.518	0.063	0.715
iC4	408.1	36.48	0.176	13.492	0.081	0.752
nC4	425.2	38	0.193	14.06	0.081	0.777
iC5	460.4	33.84	0.227	18.511	0.098	0.828
nC5	469.6	33.74	0.251	19.315	0.1	0.864
C6	507.4	29.69	0.296	25.626	0.123	0.931
C7–C25	666.25	20.39	0.756	64.334	0.235	1.57
C26–C49	893.95	14.19	1.262	166.429	0.454	2.188
C50–C64–PN	956.95	13.72	1.313	197.247	0.502	2.245
C65–C80–PN	1118.45	14.1	0.876	262.18	0.571	1.725
C50–C80–A	1286.75	18.11	1.274	270.181	0.512	2.201

Table A4: k_{ij} interaction parameters [8] for SRK-EOS[26]. The interaction parameters not included in the table correspond to a zero value:

	N2	CO2	H2S	C50–C80–A
N2	-	0	0	0.08
CO2	-0.032	-	0	0.1
H2S	0.17	0.099	-	0
C1	0.028	0.12	0.08	0.017
C2	0.041	0.12	0.085	0.017
C3	0.076	0.12	0.089	0.017
iC4	0.094	0.12	0.051	0.017
nC4	0.07	0.12	0.06	0.017
iC5	0.087	0.12	0.06	0.017
nC5	0.088	0.12	0.069	0.017
C6	0.08	0.12	0.05	0.017
C7–C25	0.08	0.1	0	0
C26–C49	0.08	0.1	0	0
C50–C64–PN	0.08	0.1	0	0
C65–C80–PN	0.08	0.1	0	0

Case 3:

Table A5: Pure compound parameters [8]. PR76-EOS [25]

Component	Tc(K)	Pc(bar)	w	ac(bar*L2/mol2)	b(L/mol)	m
N2	126.2	33.94	0.04	1.483	0.024	0.436
CO2	304.2	73.76	0.225	3.966	0.027	0.708
C1	190.6	46	0.008	2.496	0.027	0.387
C2	305.4	48.84	0.098	6.036	0.04	0.523
C3	369.8	42.46	0.152	10.18	0.056	0.603
iC4	408.1	36.48	0.176	14.431	0.072	0.638
nC4	425.2	38	0.193	15.039	0.072	0.662
iC5	460.4	33.84	0.227	19.799	0.088	0.711
nC5	469.6	33.74	0.251	20.66	0.09	0.745
C6	507.4	29.69	0.296	27.409	0.111	0.807
C7–C25	691.81	19.46	0.68	77.739	0.23	1.299
C26–C49	956.77	13.08	1.208	221.216	0.473	1.844
C50–64PN	1118.6	10.66	0.949	371.024	0.679	1.595
C65–C80PN	1325.03	10.28	0.182	539.843	0.834	0.647
C50–C80A	1445.73	17.3	1.274	381.889	0.541	1.901

Table A6: k_{ij} interaction parameters [8] for PR76-EOS [25]. The interaction parameters not included in the table correspond to a zero value:

	N2	CO2	C50–C80A
N2	-	0	0.08
CO2	-0.032	-	0.1
C1	0.028	0.12	0.017
C2	0.041	0.12	0.017
C3	0.076	0.12	0.017
iC4	0.094	0.12	0.017
nC4	0.07	0.12	0.017
iC5	0.087	0.12	0.017
nC5	0.088	0.12	0.017
C6	0.08	0.12	0.017
C7–C25	0.08	0.1	0
C26–C49	0.08	0.1	0
C50–64PN	0.08	0.1	0
C65–C80PN	0.08	0.1	0

Appendix B: Correspondence between data sets or predicted phase diagrams in other publications in the literature, not taken as reference cases, and the topologies in the proposed classification.

Table B1 shows some correlations between the topologies presented in this work and experimental data from the literature. Although the availability of experimental information is limited and within a narrow range of pressure and temperature, it can be inferred that compositional variation in the examples shown, such as the injection of a light gas into a crude oil, modifies the AOP-line in the same way as the fluid does when modeled. Furthermore, the injection of light gas, both from an experimental and modeling perspective, leads, under appropriate conditions, to a topological transformation of the studied isopleth. Although it is not possible to describe the type of transition that occurs by observing the experimental data given their limited range, thermodynamic models allow us to infer how the topology of the isopleth will change when its composition is modified.

Table B1: Phenomenological between in this work and experimental data / calculated diagrams extracted.

Transition in this Work	Reference:	Figure at the cited reference:
Figures 5 and 6 (case 2 and 3; CH4 injection) Type II <-> type IV and Type I <-> type III respectively.	Arya et al (2016) [13]:	Figure 3 (a,b,c,d). Fluid-1: +5%, +10%, +15%, +30% gas injection respectively (GI with 71.312% of CH4) Figure 6 (a,b,c). Fluid-2: 10%, 15%, 30% gas injection respectively (GI with 87.449% of CH4) Figure 8 (d). Fluid-3: 10% CH4 injection.
	Abutaqiya et al (2020) [30]	Figure 3 (a,b,c,d). Sample Live U8, U8+10%, U8+20%, U8+30% Hydrocarbon (HC) gas injection respectively (HC with 73.54% of CH4) Figure 4 (a,b,c,d). Sample S1: S1+5%, S1+10%, S1+15%, S1+30% Hydrocarbon (HC) gas injection respectively (HC with 71.31% of CH4) Figure 7 (a,b,c,d). Sample Live S14(S14), S14+5%, S14+10%, S14+20%, Hydrocarbon (HC) gas injection respectively (HC with 60.57% of CH4)
	Panuganti et al (2012) [11]	Figure 3 (a,b,c,d). Crude B: B+0%, B+5%, B+15%, B+30% gas injection (GI) respectively (GI with 71.4% of CH4). Figure 4 (a,b,c,d). Crude C: C+0%, C+10%, C+15%, C+30% gas injection (GI) respectively (GI with 87.4 % of CH4).
Figure 7, case 2 (CO2 injection) Type II <-> type IV	Arya et al (2016) [13]:	Figure 8 (c). Fluid-3: 10% CO2 injection.

Abutaqiya et al (2020) [30]	Figure 6 (a,b). Sample B7: B7+20%, B7+30% CO2 injection respectively.

Appendix C: Phase envelopes tracing methodology

The tracing of two-phase lines in the solution of the equilibri conditions:

$$F = \begin{bmatrix} lnK_1 + ln\hat{\varphi}_1^V - ln\hat{\varphi}_1^L \\ \cdots \\ lnK_i + ln\hat{\varphi}_i^V - ln\hat{\varphi}_i^L \\ \cdots \\ lnK_N + ln\hat{\varphi}_N^V - ln\hat{\varphi}_N^L \\ \sum_{i=1}^{N}(y_i - x_i) \\ X_S - S \end{bmatrix} = \vec{0}$$

Where K_i is the ient between the vapor and liquid phases molar fractions:

$$K_i = \frac{y_i}{x_i}$$

The set of variables of this sy

$$X = \begin{bmatrix} lnK_1 \\ \cdots \\ lnK_i \\ \cdots \\ lnK_N \\ lnP \\ lnT \end{bmatrix}$$

Where X_S is a specified variable (for example, pressure) and S is the value of specification for that specified variable to solve at a particular point. This system of equations is solved for each point with a Newton-Raphson method, ending up in the system [17]:

$$X = \begin{bmatrix} lnK_1 \\ \cdots \\ lnK_i \\ \cdots \\ lnK_N \\ lnK_1^S \\ \cdots \\ lnK_i^S \\ \cdots \\ lnK_N^S \\ lnP \\ lnT \\ \beta \end{bmatrix} \quad F = \begin{bmatrix} lnK_1 + ln\hat{\varphi}_1^V - ln\hat{\varphi}_1^L \\ \cdots \\ lnK_i + ln\hat{\varphi}_i^V - ln\hat{\varphi}_i^L \\ \cdots \\ lnK_N + ln\hat{\varphi}_N^V - ln\hat{\varphi}_N^L \\ lnK_1^S + ln\hat{\varphi}_1^L - ln\hat{\varphi}_1^{L2} \\ \cdots \\ lnK_i^S + ln\hat{\varphi}_i^L - ln\hat{\varphi}_i^{L2} \\ \cdots \\ lnK_N^S + ln\hat{\varphi}_N^L - ln\hat{\varphi}_N^{L2} \\ \sum_{i=1}^N (y_i - x_i) \\ \sum_{i=1}^N (w_i - x_i) \\ X_S - S \end{bmatrix} = \vec{0}$$

Which is solved with the same procedure as the two-phase lines.
The tracing of the whole phase diagram can be divided in three steps:

- Two-phase envelopes tracing
- Detection of double saturation points (crossings)
- Three-phase envelopes tracing

In the first step, the AOP line is traced, starting from a low-temperature dew point. If this line goes to high pressure then the bubble points line is calculated, starting from low temperature. After both lines are calculated, a crossings check is made which will determine how to calculate the three-phase regions.

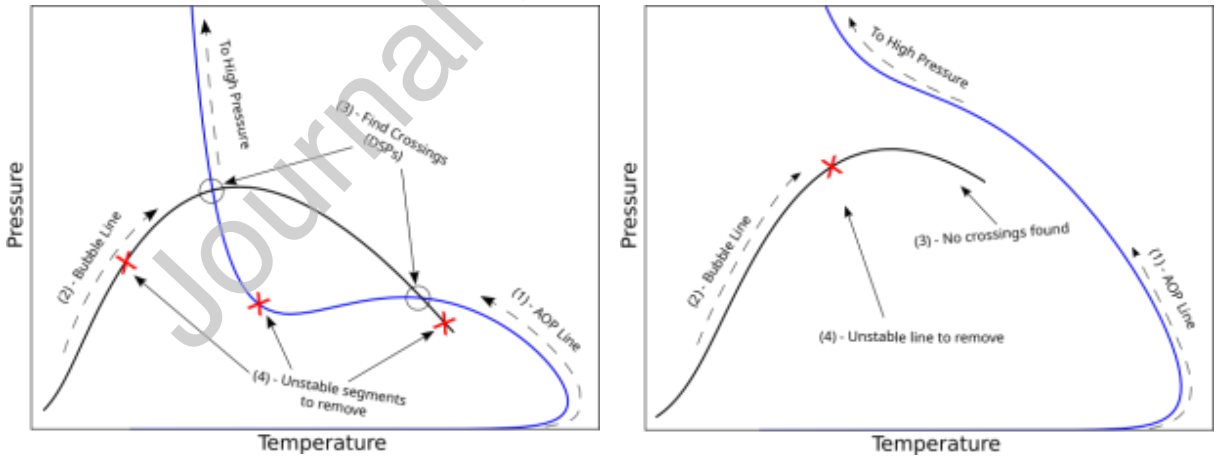

Fig. C1 Two phase envelopes tracing, detection of DSPs and removal of unstable regions.

A more unusual scenario is when the dew line ends at low pressure instead of diverging towards high pressure. Then, in this case, a high-pressure liquid-liquid equilibrium line is calculated and finally, the bubble line starting from low temperature. After the three lines are calculated, crossings between them are found.

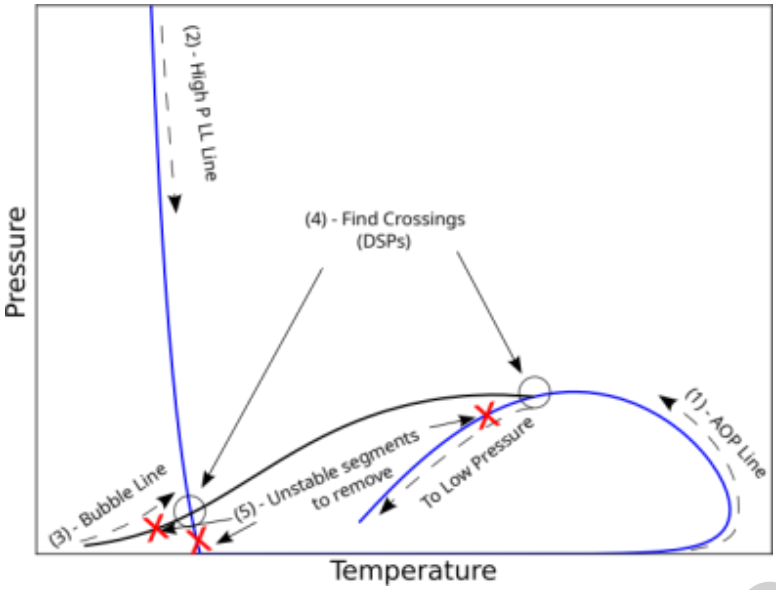

Fig. C2 Two phase envelopes tracing, detection of DSPs and removal of unstable regions, for the special case where the dew/AOP line ends at low pressure.

If DSPs were found, three-phase lines are calculated from each existent DSP. If no DSP was found, then the isolated three-phase lines are traced [17].

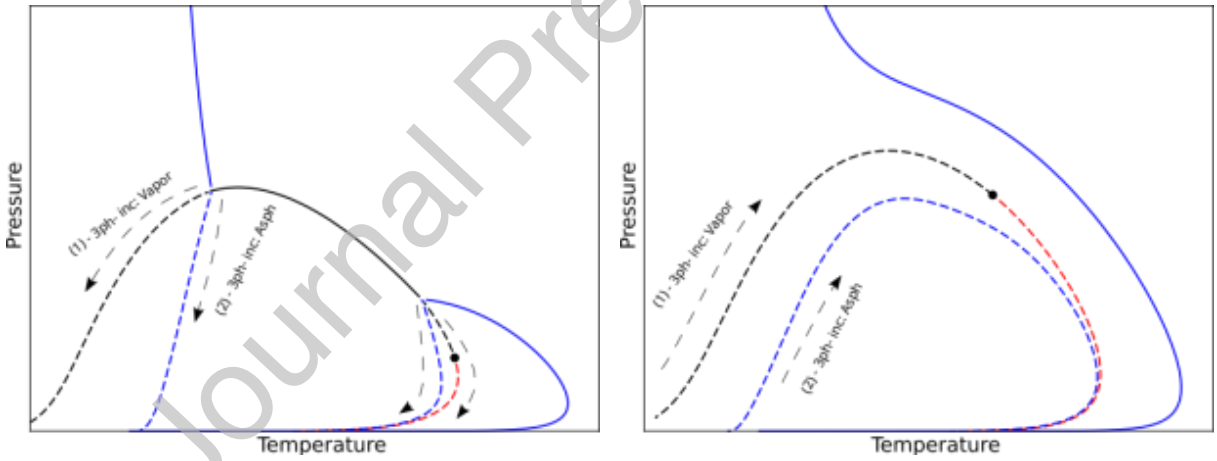

Fig. C3 Tracing of three phase envelopes.

Appendix D: Influence of k_{ij} between H_2S and asphaltenes on phase diagram type transition by injection.

On the original Case 2 characterization extracted from literature, a null k_{ij} between H_2S and asphaltenes was used. Here we show how this parameter could affect the predicted phase diagram and also the types transitions by injection of gas at different k_{ij} values.

k_{ij} influence on a single composition

In Fig. D1 it can be seen how the values of k_{ij} directly impact the asphaltenes onset lines. Whereas its values increase the upper AOP line gets higher and the lower AOP gets lower, giving larger regions where there is the presence of an asphaltenic phase. It is also important to remark how the bubble curves (either two or three-phase boundaries) remain unaltered by changes in k_{ij}.

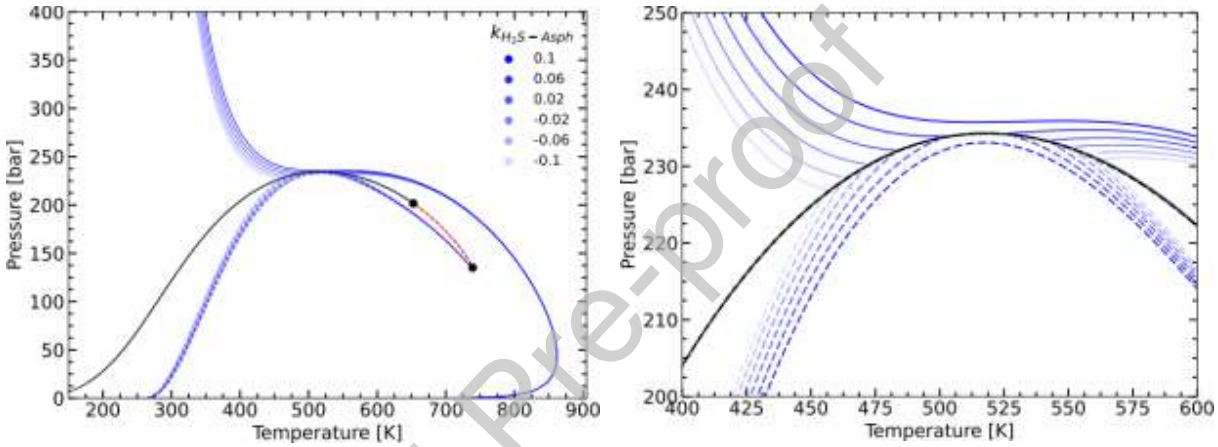

Fig D1: k_{ij} influence at a single composition

k_{ij} influence on the transition of phase diagram type

Here it is shown that the k_{ij} value can influence the transition between types of phase diagrams. Figures D2 to D4 present the effect of injections in three different parametric scenarios, one with negative k_{ij} (-0.1), the original case with null k_{ij}, and one with positive k_{ij} (0.1). In the case of negative k_{ij}, the injection of H_2S shows a more pronounced crossover while it disappears at positive values. This implies that, for injections of H_2S, negative k_{ij} values favor transitions IV → II since one side of the AOP line will always decrease in pressure eventually reaching the three-phase region and resulting in two DSPs. Meanwhile, positive values of k_{ij} favor transitions II → IV since the AOP always gets higher as the H_2S increases.

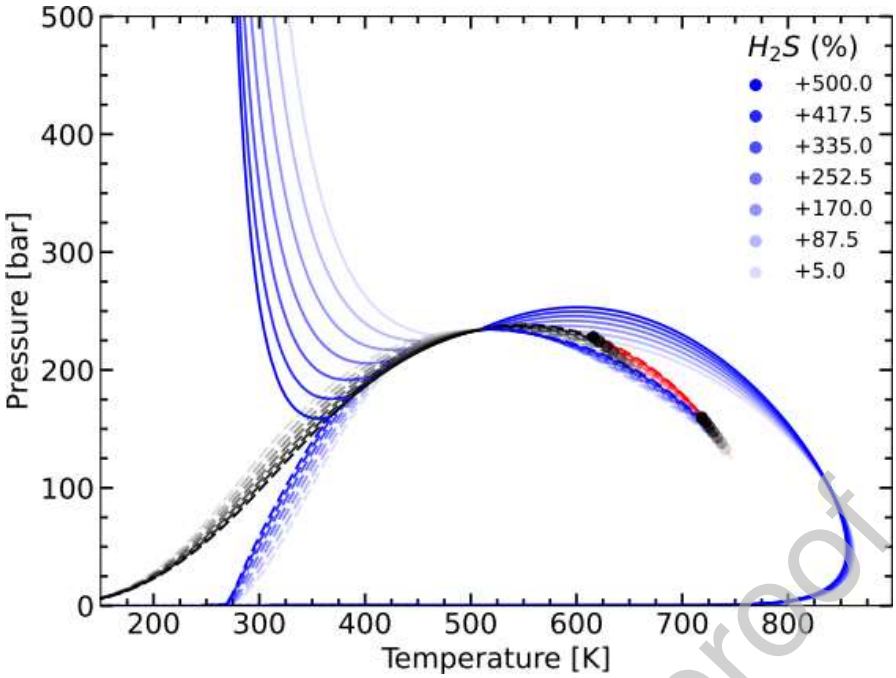

Fig D2 Negative k_{ij} (-0.10) influence for an injection of H_2S

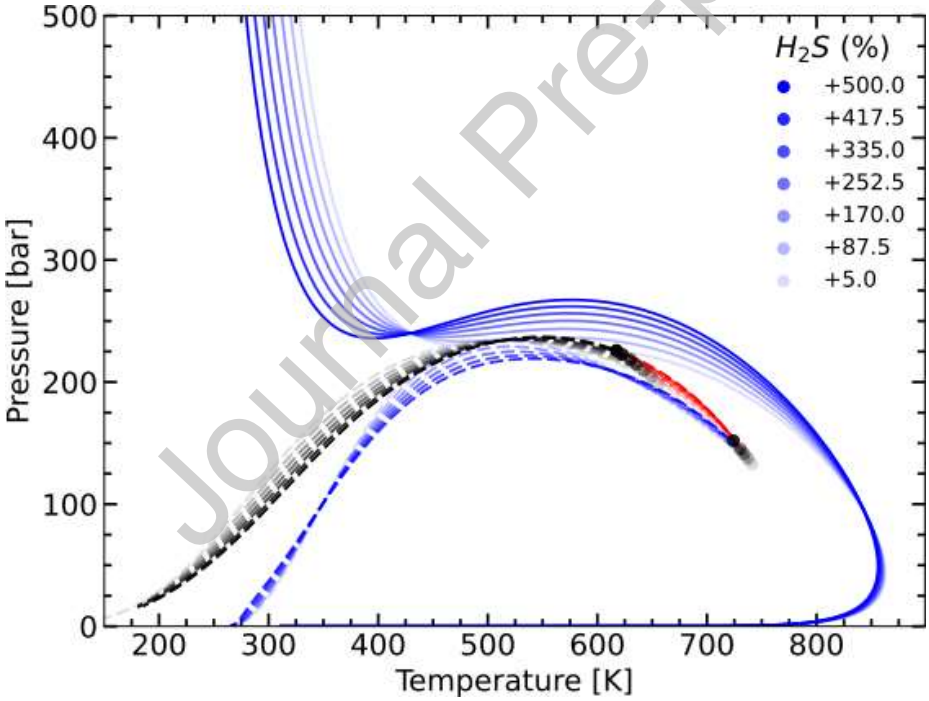

Fig D3 Null k_{ij} influence for an injection of H_2S

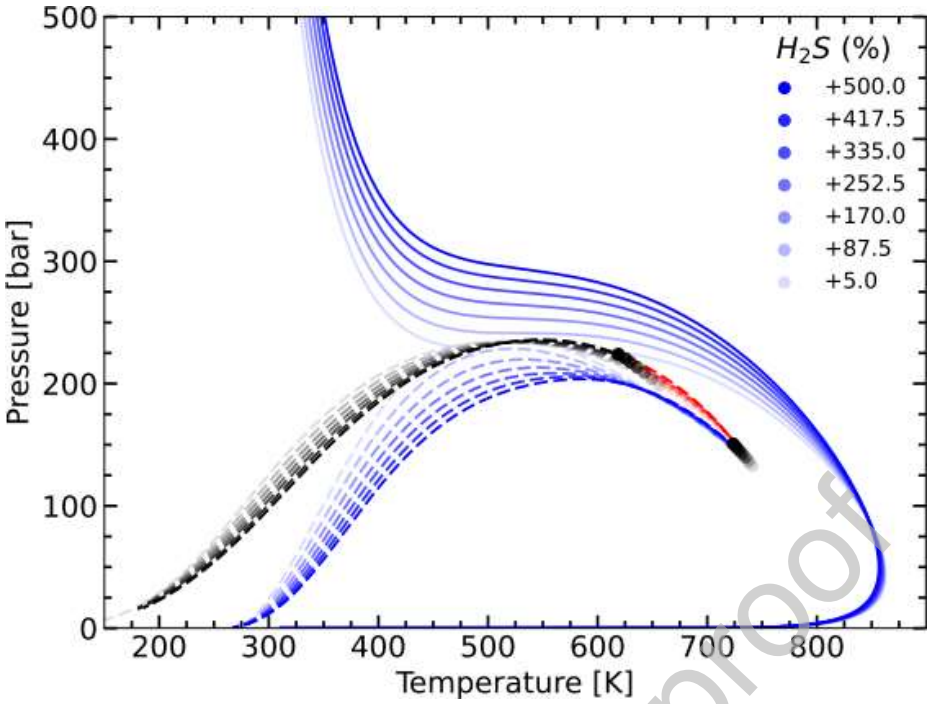

Fig D4 Positive k_{ij} (0.10) influence for an injection of H_2S

Appendix E: Alternative lumping strategies for Case 3

Table E1 Lumping with 8 pseudo-components + asphaltenes.

Component	z	Tc(K)	Pc (bar)	w	Exponential w
C7-C15	0.15850	619.97	21.91	0.51	0.51
C16-C25	0.06938	775.27	15.49	0.88	0.89
C26-C37	0.02856	917.16	13.44	1.18	1.17
C38-C49	0.00872	1057.92	12.53	1.27	1.37
C50 - C57	0.00210	1091.31	11.05	1.05	1.55
C58 - C64	0.00087	1196.58	10.85	0.74	1.62
C65-C72	0.00048	1296.73	10.71	0.35	1.67
C73-C80	0.00022	1403.09	10.61	0	1.7
C50-C-80 A	0.00086	1445.73	17.07	1.27	1.27

Table E2 Lumping of 4 pseudo-components + asphaltenes

Component	z	Tc(K)	Pc (bar)	w	Exponential w
C7–C25	0.22738	691.07	18.97	0.68	0.68
C26–C49	0.03747	959.3	13.17	1.208	1.23
C50–C64–PN	0.00230	1125.17	10.99	0.949	1.57
C65–C80–PN	0.00054	1332.51	10.68	0.182	1.68
C65–C80–A	0.00086	1445.73	17.07	1.274	1.27

Table E3 Lumping with 2 pseudo-components + asphaltenes.

Component	z	Tc(K)	Pc (bar)	w	Exponential w
C7-C43	0.26206	758.28	17.44	0.82	0.82
C44-C80	0.00676	1143.17	11.5	0.96	1.52
C50-C-80 A	0.00086	1445.73	17.07	1.27	1.27

Table E4 Lumping with 1 pseudo-component + asphaltenes.

Component	z	Tc(K)	Pc (bar)	w	Exponential w
C7-C80	0.26882	789.39	16.96	0.83	0.88
C50-C-80 A	0.00086	1445.73	17.07	1.27	1.27

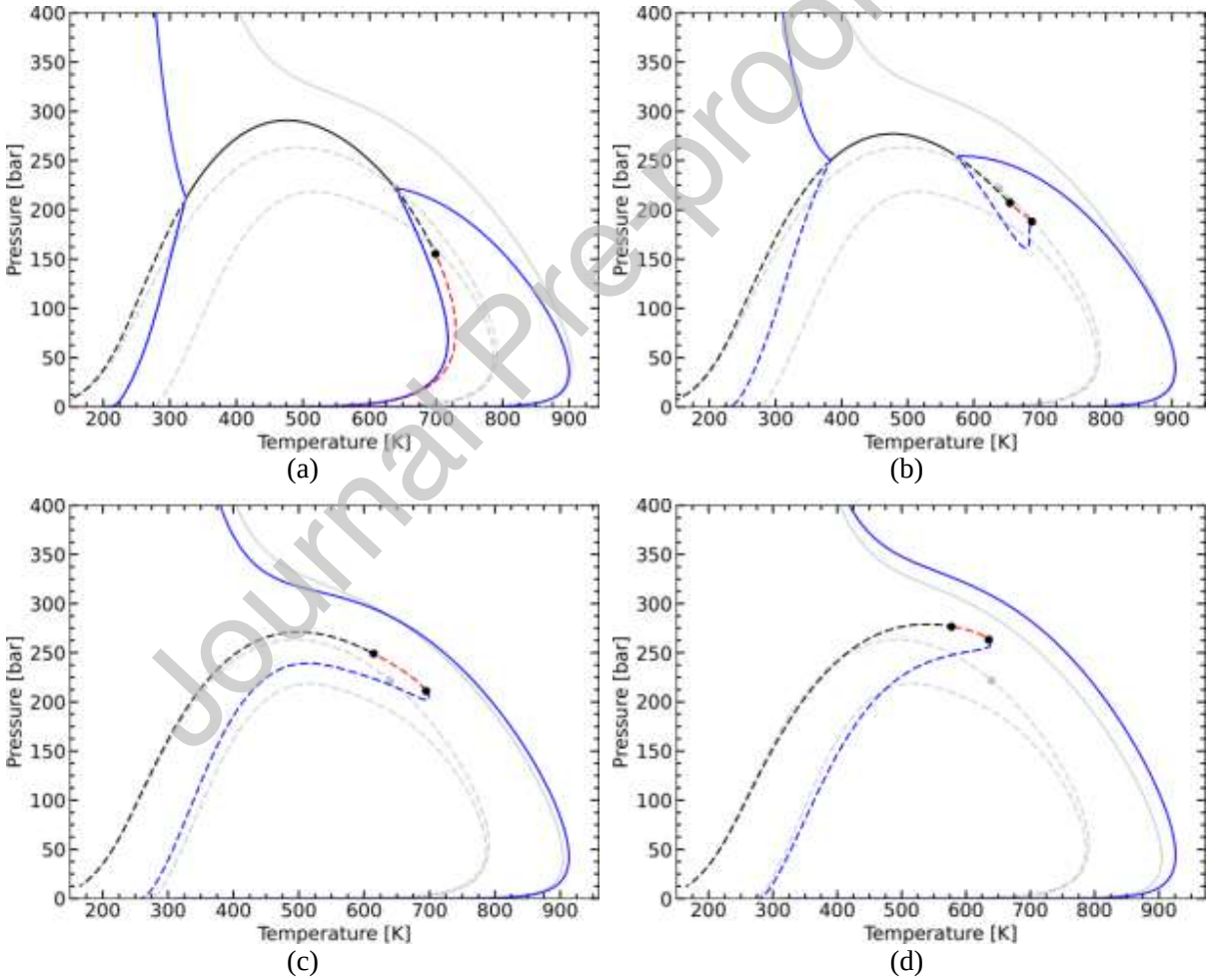

Fig. E1 Revisited lumping strategy with an exponential correlation for the acentric factor, compared with the original Case 3 with the original correlation. (a): Lumping of 1 pseudo-component + asphaltenes., (b): Lumping of 2 pseudo-components + asphaltenes, (c): Lumping of 4 pseudo-components + asphaltenes and (d): Lumping of 8 pseudo-component + asphaltenes

Graphical abstract

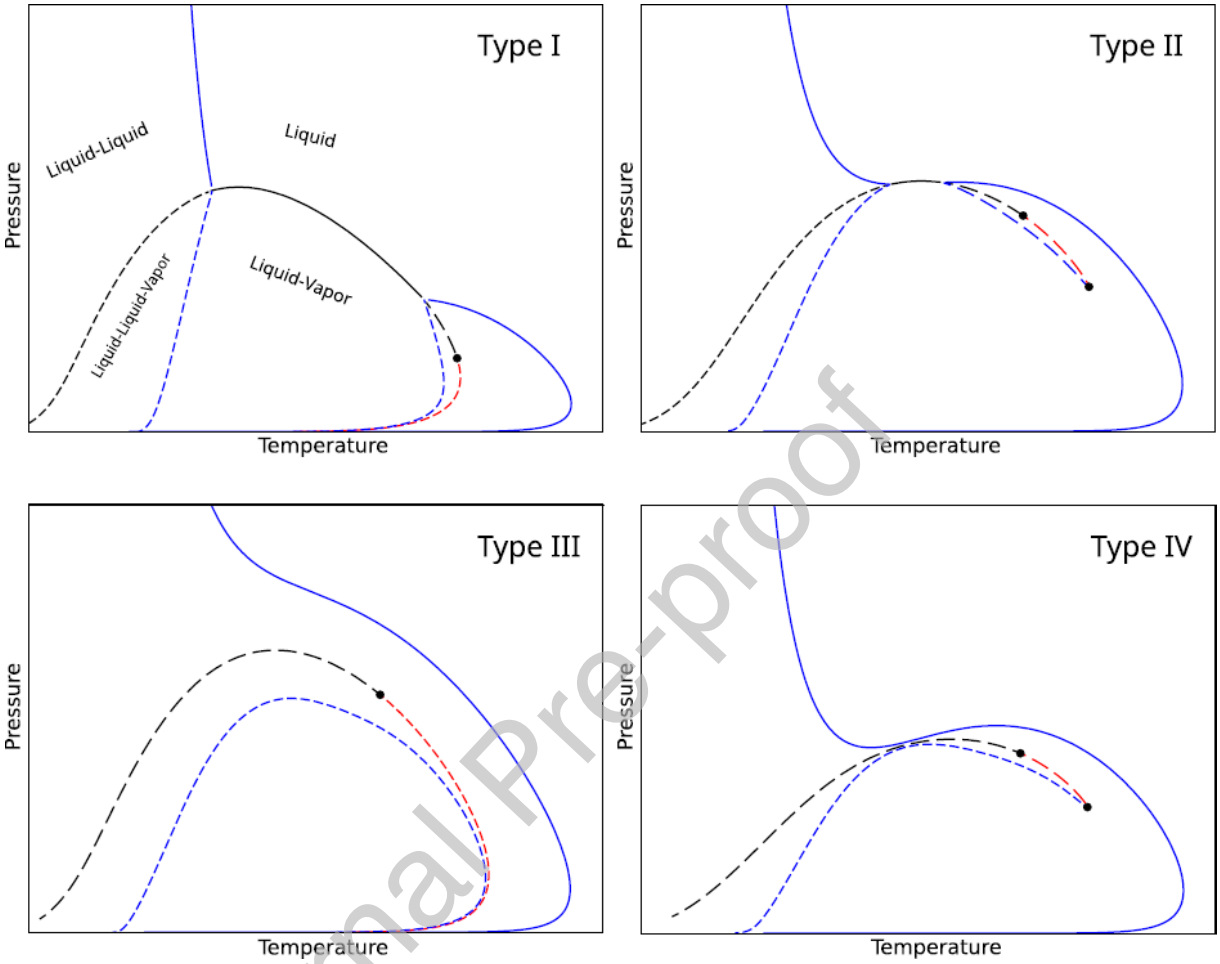

Federico Ezequiel Benelli: Investigation, Methodology, Data curation, Formal analysis, Software, Validation, Visualization, Writing- Original draft preparation. **Gerardo Oscar Pisoni**: Investigation, Data curation, Formal analysis, Validation, Writing- Original draft preparation. **Martín Cismondi-Duarte**: Conceptualization, Software, Methodology, Resources, Supervision, Writing- Original draft preparation, Writing- Review & Editing.

Declaration of interests

☒The authors declare that they have no known competing financial interests or personal relationships that could have appeared to influence the work reported in this paper.

☐The authors declare the following financial interests/personal relationships which may be considered as potential competing interests: